GPS BASED TECTONIC ANALYSIS OF THE ALEUTIAN ARC AND BERING PLATE

By

Ryan S. Cross

RECOMMENDED:

Wesley K Wallace

Douglas H Christensen

Advisory Committee Chair

Michael E. Wiest

Chair, Department of Geology and Geophysics

APPROVED:

Dean, College of Natural Science and Mathematics

Susan M. Henrichs

Dean of the Graduate School

April 6, 2007

Date

GPS BASED TECTONIC ANALYSIS OF THE ALEUTIAN ARC AND BERING PLATE

A

THESIS

Presented to the Faculty

of the University of Alaska Fairbanks

in Partial Fulfillment of the Requirements

for the Degree of

MASTER OF SCIENCE

By

Ryan S. Cross, B.S.

Fairbanks, Alaska

May 2007

Abstract

Global Positioning System (GPS) measurements enable a quantitative analysis of tectonic deformation in the Aleutian Islands, Alaska. We construct elastic deformation models to calculate coupling on the subduction interface and the interseismic strain recorded at stations throughout the Aleutian arc. Using a grid-search inversion procedure, we determine an arc translation velocity for each region of the arc, revealing south to southwest motions of 4 to 14 mm/yr. In the central Aleutians, there is good agreement between areas of high coupling and areas of large moment release in major seismogenic events. We have combined modeling results from the Aleutians with direct measurements of station velocities of sites in western Alaska and the Bering Sea islands to test the hypothesis of a clockwise rotating Bering plate. The Bering Sea area including the Aleutian arc and western Alaska is fit by an Euler pole located at 42.5° N, 121.3° E with an angular velocity of 6.0°/my, relative to stable North America. The Bering plate's eastern boundary appears to be related to left lateral faulting in interior Alaska as clockwise rotation of the plate results in south-southwest motion relative to the North American plate. The Bering plate's interaction with a counter-clockwise rotating southcentral Alaska block may be responsible for the decreased slip-rate on the western Denali fault. Thrust earthquake slip azimuths expose a systematic discrepancy with Pacific-Bering plate convergence direction. A simple model of slip partitioning and GPS measurements reveal that slip partitioning is present in the forearc throughout the arc but only develops in the back arc west of Amchitka Pass.

Table of Contents

Page

Page

Page

List of Figures

Page

Page

List of Tables

Page

List of Other Material

List of Appendices

Page

Acknowledgements

First, I would like to thank my advisor Dr. Jeff Freymueller. Not only did Jeff provide me with a remarkable project to work on, but he has guided me through this masters program is a way that has been both challenging and enjoyable. I would like to thank my committee members Dr. Doug Christensen and Dr. Wes Wallace for their review of my thesis and for being excellent instructors.

I thank my office mates Julie Elliott, Tom Fournier, Samik Sil, Jill Shipman, Chris Larsen, and Mike Thorne for all their great advice and help with matlab, GMT, fieldwork and more.

A special thanks to Max Kaufman. Max is the man with the plan who gets the job done. I thank Max for helping me with my fieldwork but for also making all of our other fieldwork adventures enjoyable and productive. I wish to thank all the people who have helped to collect the data used throughout this thesis, including many of Jeff's previous students, and other researchers at the Geophysical Institute.

I am grateful for the funding provided for this project by the National Science Foundation, and to the Geology and Geophysics department at UAF for providing me with teaching opportunities.

I thank my parents for their support over all these years, and to my friends in Fairbanks who helped make this such a great place to live.

My final and biggest thanks go to Molly, my fiancée, for all her encouragement and for making my world a wonderful place.

Chapter 1

Introduction

1.1 General

Plate tectonics is the most unifying theory behind all geology and geophysics. The recognition of rigid tectonic plates and delineation of their boundaries has allowed for great improvements in our understanding of Earth. Plate tectonics is so fundamental to geology and geophysics that one would think that all plates that make up Earth's lithosphere already would be identified and their motions described quantitatively. However, there remains at least one significant region for which there is not agreement about the plate configuration: northeast Asia, including the Bering Sea and its margins. This region has received relatively little attention, perhaps because it is remote and surrounded by other poorly characterized areas, and because researchers were until a decade ago divided by the Iron Curtain.

Before we[1] began this study, seismicity patterns, focal mechanisms, and limited GPS data demonstrated that at least the southern Bering Sea moves significantly, relative to North America, but little else was known. *Mackey et al.* [1997] analyzed seismicity around the Bering Sea region and proposed the existence of a Bering plate comprising the Bering Sea, Aleutian arc, part of western Alaska, and parts of Chukotka and the Koryak Highlands. The pole for the Bering plate relative to North America was proposed to lie in northern Chukotka (Figure 1.1). *Fujita et al.* [2002] predicted the same sense of

[1] The word we describes the author and his advisor, Dr. Jeff Freymueller. "We" is used throughout the thesis as Chapters 2 and 3 are manuscripts written for publication.

deformation around the boundaries of the Bering plate with a similar pole location, but neither study predicted the rate of motion of the plate.

Our goal for this study was to use GPS measurements to quantitatively assess the Bering plate hypothesis. We wanted to determine not only how the Bering plate moves but also where its boundaries lie and what is driving its motion. Furthermore, we aimed to assess if the northern regions of the Bering Sea behaved differently from the Aleutian arc; in other words, we would attempt to detect motion on the far western Denali fault system.

Using GPS measurements we have addressed all of these issues and although there is much left to learn, we have to a first approximation unraveled the tectonic motions of the Bering plate and its boundaries. Figure 1.1 displays the primary findings from our study, the approximate boundaries of the Bering plate and its Euler pole.

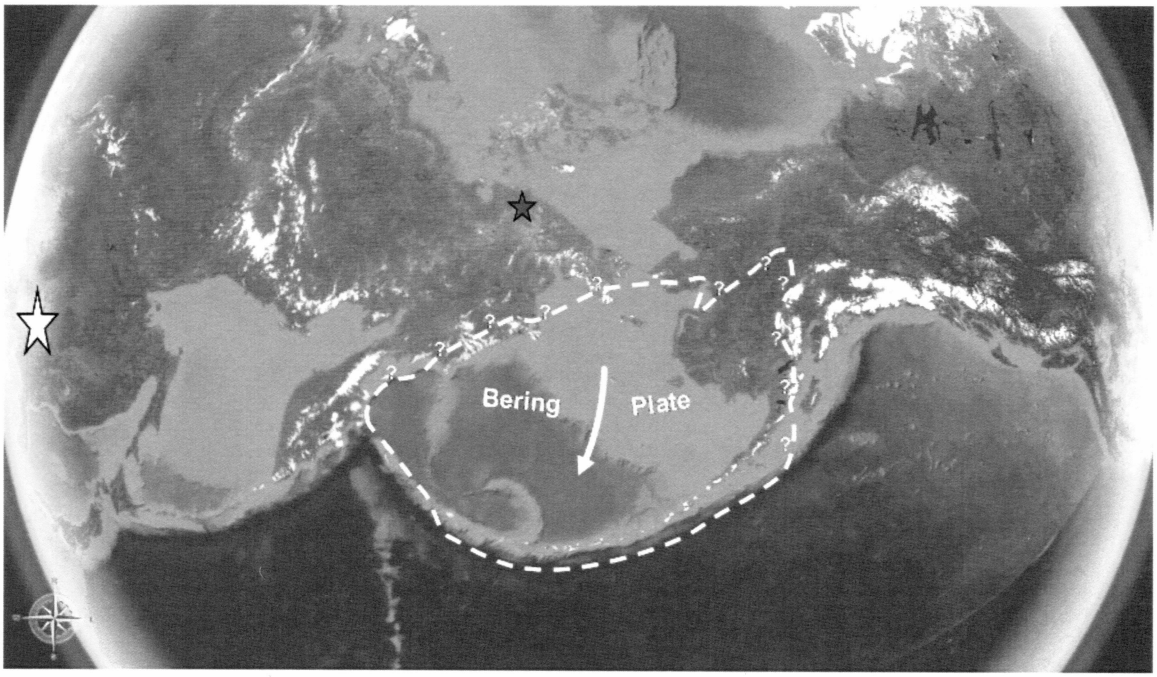

Figure 1.1 Bering plate and Euler pole location. This image is a synthetic view of Earth from an altitude of 4500 km showing the approximate boundaries of the Bering Plate. The white star indicates the location of the Bering plate Euler pole (relative to North America) determined using GPS. The green star indicates the predicted Euler pole location based on seismicity [*Mackey et al.*, 1997]. Dashed line with question marks denotes regions where the plate's boundaries are inferred. Note that the eastern half of the plate is composed of continental crust (light blue and green) and the western half is oceanic crust (darker blue). Background image from *World Wind.*

1.2 Thesis Content and Organization

This thesis consists of two main self-contained chapters along with this introduction and a general conclusions section. Bibliographies containing references for each chapter are listed at the end of each chapter, as are relevant appendices.

Chapter 2 was published in *Geophysical Research Letters* in March 2007. This paper focuses on the Andreanof Islands region of the Aleutian arc. Here the Pacific plate subducts obliquely beneath the overriding crust causing interseismic deformation that has been recorded with GPS. This chapter focuses on using the methods of elastic dislocation modeling to remove the components of interseismic strain from the GPS observations, revealing the long-term motion of the arc (arc translation rate). In developing our dislocation model, we have determined the coupling on the subduction interface and examined similarities between regions of high coupling and areas of large moment release in major earthquakes.

In Chapter 3 we extend our methods of elastic dislocation modeling to other regions of the Aleutian arc to determine the arc translation rates. Chapter 3 is the heart of this thesis and along with quantitatively analyzing the Bering plate, we explore many implications regarding the boundaries of the plate. One difference between Chapters 2 and 3 is that in Chapter 3 we use an improved definition of the motion of the North American plate in our geodetic reference frame. This changes the velocities relative to North America by ~2 mm/yr, which changes the estimated velocities of the Aleutian arc and Bering plate.

Much of the effort in this research was in developing the *Matlab* scripts used in elastic dislocation modeling; therefore, it is only appropriate that this material be included in its most relevant form. I have included a CD that contains these Matlab scripts and the associated files needed to execute the scripts. For more information regarding the files and their use, please see the README text file located on the CD.

1.3 References

Mackey, K., K. Fujita, L. Gunbina, V. Kovalev, V. Imaev, B. Koz'min, and L. Imeava (1997), Seismicity of the Bering Strait region: Evidence for a Bering block, *Geology*, 25(11), 979-982.

Fujita, K., K. G. Mackey, R. C. McCaleb, L. V. Cunbina, V. N. Kkovalev, V. S. Imaev, and V. N. Smirnov (2002), Seismicity of Chukotka, northeastern Russia, in: Tectonic evolution of the Bering shelf-Chukchi Sea-Arctic margin and adjacent landmasses, ed. By Miller, E. L., A. Grantz, and S. L. Klemper, *Geol. Soc. Amer. Spec. Pap.*, 360, 259-272.

Chapter 2

Plate Coupling Variation and Block Translation in the Andreanof Segment of the Aleutian Arc Determined by Subduction Zone Modeling Using GPS Data[2]

2.1 Abstract

We use GPS measurements in the first geodetic study of plate coupling on the Andreanof segment, Aleutian subduction zone. The Pacific plate subducts obliquely at a rate of 7.3 cm/yr resulting in northwestward displacements greater than 1 cm/yr at stations located on the west end of the Andreanof region, but velocities at the east end are smaller in magnitude and oriented west-southwest. These velocity variations are caused by differences in plate coupling along the subduction zone, which correlate with the rupture zones of the 1986 and 1996 M_w8 earthquakes. We construct a dislocation model to estimate the velocity of the arc in the Andreanof region relative to North America, and fault plane coupling coefficients. Our best model shows a southwestward velocity of 7.8 mm/yr, a high degree of coupling in the main thrust zone at the west end of the subduction zone, and little to no coupling at the east end.

---

[2] Published as Cross, R. S., and J.T. Freymueller, *Geophys. Res. Lett.,* [in press]

2.1 Introduction

We use surface velocity estimates from repeated GPS observations to study subduction zone deformation in the Andreanof Islands, Aleutian arc (Figure 2.1). Previous studies of velocities of GPS sites on Unimak and Sanak Islands and the Alaska Peninsula, ~1000 km to the northeast, show velocities of ~4 mm/yr to the southwest [*Freymueller and Beavan*, 1999; *Mann and Freymueller*, 2003]. They found little indication of strain associated with subduction, so they interpreted the velocities as a southwestward translation of those regions relative to stable North America. *Ekstrom and Engdahl* [1989] determined an arc-parallel translation velocity of the Andreanof region of 30±10 mm/yr relative to North America based on slip vector azimuths for thrust earthquakes from the Aleutian arc. Displacements recorded on the Andreanof Islands can be broken into two parts, a part that is caused by coupling in the subduction zone and a part due to the steady translation of the arc relative to North America. We invert the Andreanof Islands velocities to calculate the coupling on the subduction zone interface using dislocation modeling techniques while also solving for the translation velocity of the Andreanof region relative to North America.

This tectonically and seismically active region of the Aleutian arc has ruptured in three major earthquakes over the last 50 years. The 1957 (M_w 8.6) earthquake ruptured the Andreanof segment of the Aleutian arc and propagated east 600 km to the Unalaska region [*Taber et al.*, 1991]. The 1986 Andreanof Islands earthquake (M_w 8.0) and the 1996 event (M_w 7.9) again ruptured the western one-third of the 1957 rupture area. The

1996 rupture area included the region west of the Andreanof Islands and overlapped the western one-third of the 1986 rupture area [*Tanioka and Gonzalez,* 1998] (Figure 2.1).

The 1986 earthquake was extensively studied. *Engdahl and Gubbins* [1987] combined data from local and teleseismic stations to simultaneously solve for earthquake locations and a subduction zone velocity structure in the central Aleutian Islands. Further studies by *Engdahl et al.* [1989] and *Ekstrom and Engdahl* [1989] established that the main thrust zone that ruptured could be represented by two planes. The first plane ranges from 57 to 92 km from the trench and extends from 15 to 28 km in depth; the second plane continues from a distance of 92 km to 128 km from the trench and has a depth of 28 to 47 km. *Ekstrom and Engdahl* [1989] inferred there was little or no coupling between the subducting slab and the overriding crust in the forearc wedge, based on the lack of seismicity there.

2.3 GPS Data

We measured GPS velocities of sites on four islands: Kanaga, Adak, Great Sitkin, and Atka. Kanaga and Great Sitkin are volcano-monitoring networks; our observations revealed that sites on Great Sitkin and one site on Kanaga could not be used in this study because a small volcanic signal was present in the data. Most sites were surveyed two to four times over a 6 to 7 year time span (Appendix 2.1).

We used the GIPSY/OASIS II software version GOA4 to obtain daily coordinate and covariance estimates of our stations and regionally distributed stations in the ITRF2000 reference frame [e.g., *Freymueller et al.,* 2000]. We estimated site velocities

in ITRF2000, and then converted to velocities relative to the North America plate using the REVEL2000 model of *Sella et al.,* [2002]. The velocities and uncertainties relative to stable North America are given in Table 2.1.

Table 2.1 Site velocities relative to stable North America in mm/yr. Note that site coordinates are listed in Appendix 1.1. Sites are grouped by islands in the following order: Kanaga, Adak, and Atka.

Site Name	East Rate	East σ	North Rate	North σ	Vertical Rate	Vertical σ	Trench Normal Distance	Horizontal Rate	Horz. σ	Orientation
	mm/yr	mm/yr	mm/yr	mm/yr	mm/yr	mm/yr	Km	mm/yr	mm/yr	degrees
GATE	-9.75	0.46	6.32	0.36	8.75	0.88	155	11.62	0.58	303.0
KICM	-9.43	3.73	7.54	2.17	-1.34	5.14	163	12.07	4.32	308.6
KIRH	-9.5	0.77	6.96	0.55	-0.71	1.5	160	11.78	0.95	306.2
ROE2	-10.54	0.38	8.06	0.31	6.23	0.7	145	13.27	0.49	307.4
MIDK	-11.41	0.4	7.72	0.33	5.38	0.76	146	13.78	0.52	304.1
AT18	-11.61	0.61	6.66	0.44	7.18	1.15	152	13.38	0.75	299.8
BED1	-10.33	0.29	6.65	0.27	3.03	0.52	153	12.29	0.40	302.8
BETT	-11.35	0.62	6.55	0.44	3.5	1.26	147	13.10	0.76	300.0
BR6	-12.42	3.81	5.38	1.45	3.2	3.96	153	13.54	4.08	293.4
BUGS	-10.56	0.48	6.76	0.38	5.32	0.95	150	12.54	0.61	302.6
CLUB	-11.14	0.46	6.49	0.36	7.46	0.9	150	12.89	0.58	300.2
FNGB	-11.61	0.56	7.28	0.41	5.61	1.09	148	13.70	0.69	302.1
J122	-11.66	2.49	6.56	1.37	2.42	3.43	153	13.38	2.84	299.4
LORA	-8.88	0.62	7.04	0.45	3.11	1.25	166	11.33	0.77	308.4
SHTG	-10.79	0.47	6.47	0.37	9.61	0.9	160	12.58	0.60	300.9
WABM	-11.16	0.5	6.97	0.39	4.9	0.97	153	13.16	0.63	302.0
WHAL	-9.64	0.36	5.71	0.31	5.39	0.69	153	11.20	0.48	300.6
ZETP	-8.9	0.59	5.98	0.42	2.46	1.15	159	10.72	0.72	303.9
ATKA	-4.07	0.26	-3.75	0.26	-1.76	0.46	173	5.53	0.37	227.3
DEC2	-4.75	0.8	-3	0.48	3.06	1.44	174	5.62	0.93	237.7
CHUN	-6	0.59	-2.78	0.44	0.69	1.16	169	6.61	0.74	245.1
PUPA	-5.57	0.68	-2.72	0.51	4.14	1.35	171	6.20	0.85	244.0
WNDA	-5.1	0.74	-2.22	0.55	0.94	1.5	167	5.56	0.92	246.5

2.4 Dislocation Model

We model strain accumulation at a subduction boundary using the elastic dislocation theory following the methods of *Okada* [1992]. The earth is represented by a uniform elastic half-space and the plate interface by one or more planar faults, and the strain accumulation rate is assumed to be constant through the interseismic period. The interseismic deformation rate is computed from the superposition of steady state subduction along the entire plate interface, and steady normal slip (back slip) in the main thrust zone at the plate convergence rate, resulting in a plate interface that has a locked main thrust zone and is slipping freely above and below this zone [*Savage,* 1983]. Appropriate strike-slip and dip-slip components are determined by the convergence direction of the subducting plate and the strike of the trench. Because the Aleutian arc may be moving relative to North America, the convergence velocity is the Pacific plate velocity minus the North American plate velocity minus the velocity of the Aleutian Arc relative to stable North America.

We extend the method of *Savage* [1983] by allowing the main thrust zone to be either fully locked or partially creeping, with the slip deficit on the interface parameterized by a coupling coefficient. The coupling coefficient is one minus the slip between the two plates expressed in terms of a unit plate convergence rate. For example, if there is no slip the coupling coefficient is one, and if the slip between the two plates is equal to the rate of plate convergence, the coupling coefficient will be zero. The coupling coefficient can represent the percentage of the total interface that is locked.

The subduction zone interface includes the 1986 and 1996 rupture zones. We use the fault plane locations specified by *Ekstrom and Engdahl* [1989] to represent this area. The rupture area is bounded with a fault plane that connects the trench to the main thrust zone and a fourth plane that extends deeper beyond the specified main thrust zone (Figure 2.1, Appendix 2.2). We refer to the faults from top to bottom as the "upper", "middle", "lower", and "bottom" planes. We construct a second set of four fault planes for the Atka region, with the strike of the planes adjusted to agree with the change in strike of the trench. The east end of the Adak planes and the west end of the Atka planes meet approximately halfway between the two networks, except for the "middle" plane which meets another 95 km to the east based on the 1986 event's moment release patterns (see Discussion). The planes extended far enough laterally to avoid end effects.

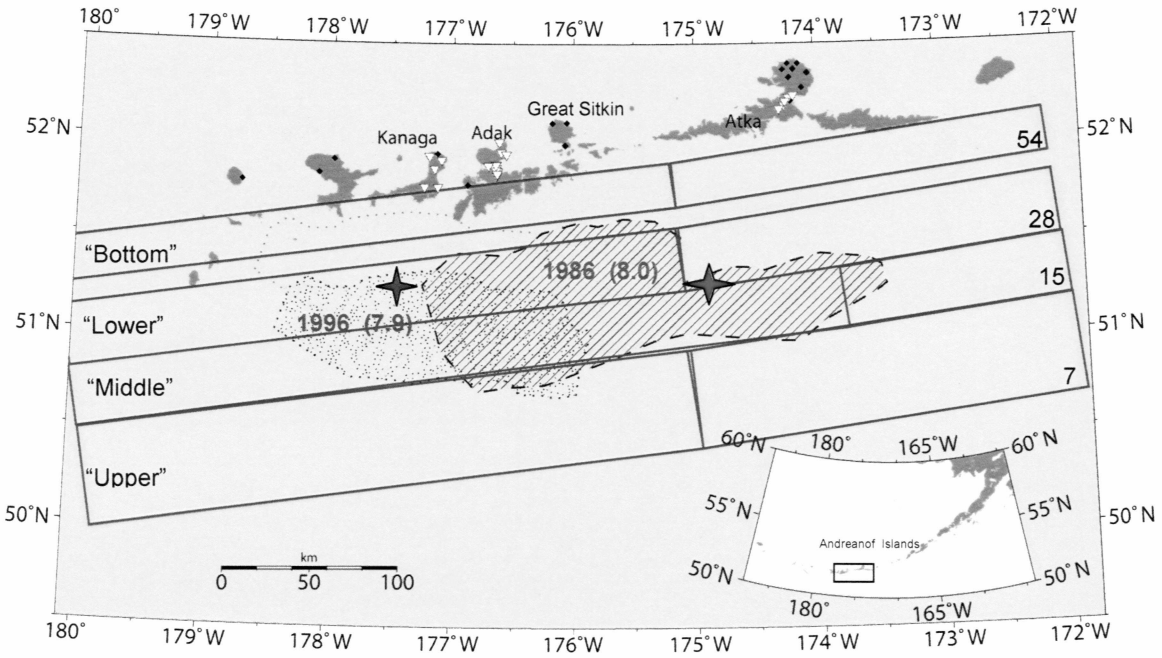

Figure 2.1 Fault plane geometry and measured velocities for the Andreanof region. Used for dislocation modeling in the Andreanof Islands region of the Aleutian subduction zone. Earthquake rupture areas are based on studies by *Engdahl and Gubbins* [1987] and *Kisslinger and Kikuchi* [1997] for the 1986 and 1996 events respectively. The 1996 rupture area has been shifted from the published location (dotted line) 40 km south based on corrections for the plate structure estimated to catalog locations determined by *Engdahl and Gubbins* [1987] for the 1986 earthquake. We assume that catalog locations for the 1996 aftershock sequence would be shifted trenchward by the same amount. Epicenters are shown as stars. Depth to the top of each set of fault planes in kilometers is shown at the east end; the top of the upper fault planes corresponds to the trench location. GPS sites are shown as inverted triangles if they are used in this study and other sites are indicated by black dots.

2.5 Inversion

Because the convergence direction depends on the (unknown) arc velocity relative to North America, the inverse model is non-linear and we solve for the arc velocity and plate-coupling coefficients using a gridded search-inversion procedure. For each candidate arc velocity, we estimate the plate coupling coefficients that minimize the overall data misfit (total χ^2). After a search over a wide range of candidate arc velocities, the model with the minimum misfit is the best overall model. We use both horizontal and vertical velocities in the inversion.

Using the assumed fault plane geometry, we calculated the 3D surface displacements at each station assuming 100% coupling on all fault planes. This generates the unit Green's functions that map the coupling on each fault plane to the displacements measured on the surface. The coupling coefficients (m) are found using a MATLAB script "lsqlin", which solves for m using linear least squares with inequality constraints. Before solving for m, the translation velocity of the arc (V_{Arc}) is subtracted from the measured velocities (d) to isolate the strain caused by the subducting Pacific plate, $d^* = d - V_{Arc}$.

This leaves d^* as displacements caused by interseismic strain accumulation. The boundary condition $0 \leq m \leq 1$ is applied to all fault planes except the bottom plane on the Adak side where m is allowed to range between -1 and 1. The negative coupling coefficient condition allows for afterslip and/or viscous relaxation that could be present below the main thrust zone due to the 1986 or 1996 earthquakes.

2.6 Results

The best-fitting model has a reduced χ^2 of 2.81 and the arc velocity is 4.1 mm/yr west and 6.7 mm/yr south (Figure 2.2a). This is equivalent to 4.9 mm/yr arc parallel (positive west) and 6.1 mm/yr arc normal (positive south), or a total velocity of 7.8 mm/yr at an azimuth of 210.3°.

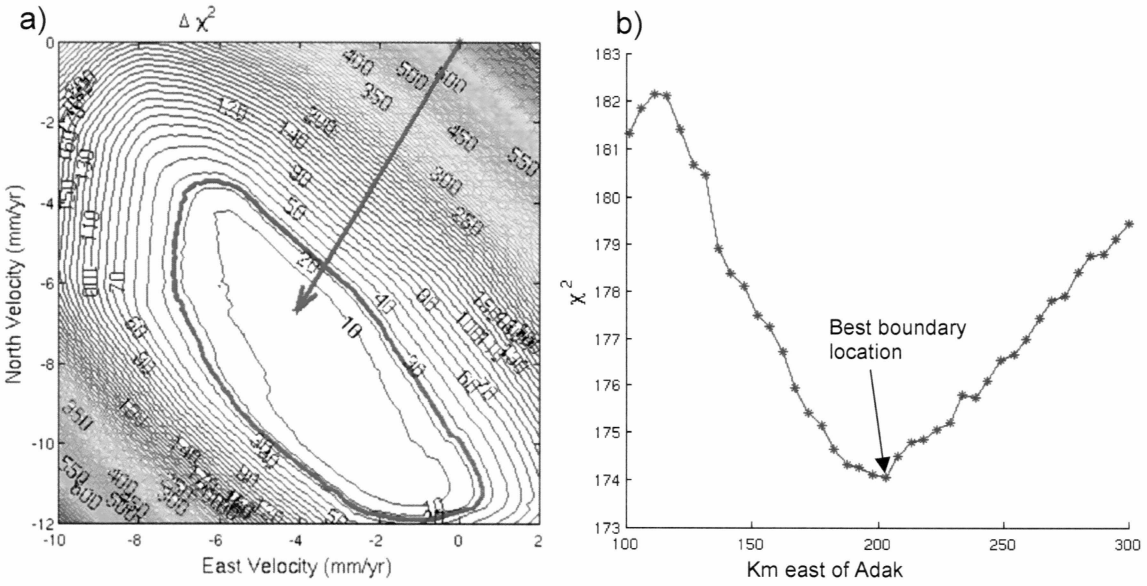

Figure 2.2 Minimum χ^2 plots for Andreanof Islands region. (a) $\Delta\chi^2$ contour plot for a range of east and north velocities of the arc in the Andreanof region. Contour lines are equally spaced at intervals of 10 above the minimum χ^2 value of 174 (4.1 mm/yr west, and 6.7 mm/yr south). The 95 % confidence region is outlined by the thick red line. (b) χ^2 vs. along strike position of the boundary between the Adak and Atka middle plane.

The coupling coefficients for the eight fault planes are shown in Figure 2.3. Our best model predicts little to no coupling in the Adak and Atka upper fault planes; this result is consistent with moment release distribution and seismicity patterns. A significant tradeoff can exist between model parameters, making the uncertainty of the coupling coefficients difficult to determine clearly. Tradeoff between the Adak bottom and lower planes allows the coupling coefficient for the bottom plate to vary between -72% and 5% while remaining within the 95% confidence region, while the coupling on the lower plane must fall between 50% and 100% (Figure 2.4). There is not a significant tradeoff between the coupling on the middle and bottom planes, which make up the main thrust zone. The best model has both parameters near their upper limits of 100%. A tradeoff can also exist between the coupling and the arc translation velocity.

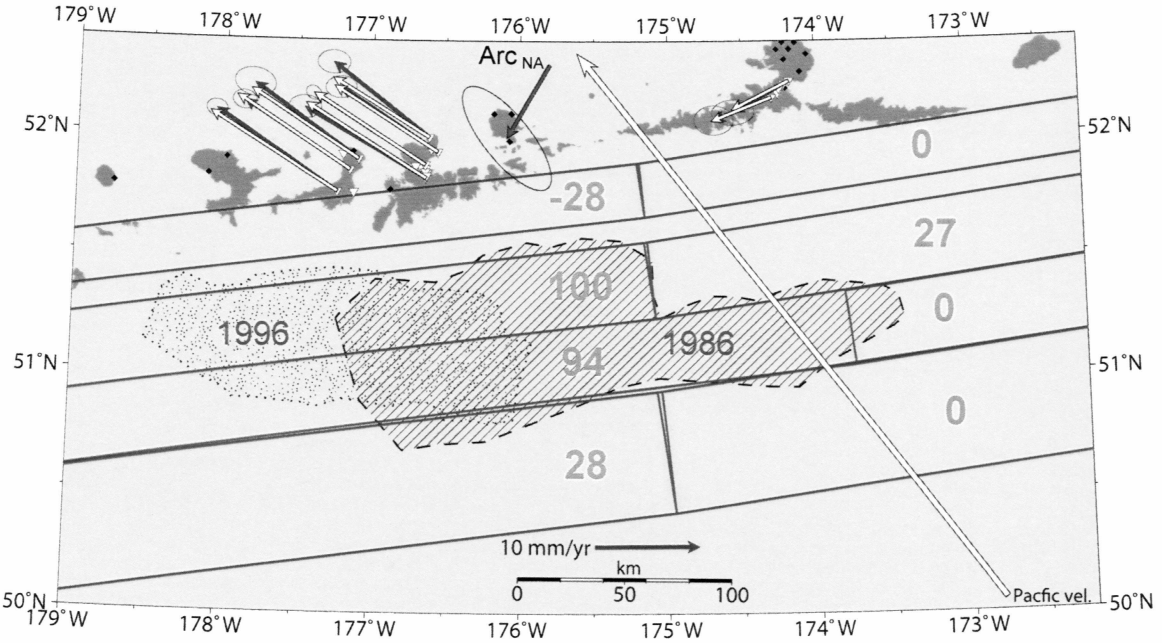

Figure 2.3 Elastic dislocation modeling results for Andreanof Islands region. Measured (blue) and modeled (white) velocities for sites located in the Andreanof region of the central Aleutians. All velocities are relative to North America. Bold pink numbers denote the percent of unit coupling for the associated fault plane. The red arrow ($Arc_{N.A.}$) is the best-fit translation velocity for the Andreanof segment. Ellipses represent 95% confidence regions. Long white arrow is the velocity of the Pacific plate relative to North America. The component of the arc velocity in the direction of Pacific plate motion is less certain because of tradeoffs between the arc velocity and plate coupling.

The bottom plane of the Adak region best fits the data with a coupling of -28% of the plate convergence rate. This may be attributed to postseismic-deformation resulting from the 1986 and 1996 earthquakes, although viscoelastic relaxation may explain this deformation better than afterslip. The 95% confidence bound on this parameter includes zero (Figure 2.4).

A strong along strike variation exists within the Andreanof segment of the Aleutian subduction zone. The thrust interface is nearly 100% locked in the western Andreanof region south of Adak from 60 to 130 km north of the trench axis, while the eastern region south of Atka is largely creeping. This variation is responsible for the along strike difference in strain determined using GPS and likely controls the extent of rupture area and moment release associated with major earthquakes.

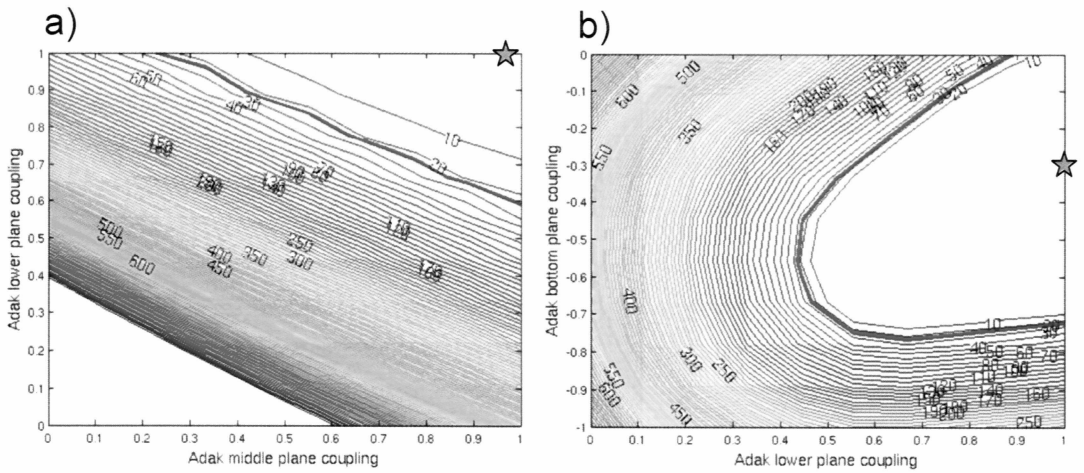

Figure 2.4 Trade-off plots showing coupling vs. $\Delta\chi^2$. The pink star indicates the minimum χ^2 location with respect to coupling coefficient values. The 95 % confidence region is outlined by the thick red line. For these figures, the arc translation velocity is allowed to vary within the 95% confidence region shown in figure 2.2a. a) shows that there is no trade off between the Adak middle and lower plane and that data are best fit when both values are near their upper bound. Figure 2.4a also demonstrates that there is greater uncertainty in the middle plane than in the lower plane as is expected because of their respective distances from the measurement locations. b) This plot demonstrates a clear trade off between coupling on the lower plane and bottom plane.

2.7 Discussion

The estimated coupling coefficients show that the parts of the fault that are locked today (high slip deficit) correspond to the rupture areas of the 1986 and 1996 earthquakes. *Houston and Engdahl* [1989] studied the spatio-temporal distribution of moment release for the 1986 Andreanof Island earthquake and found that 90% of the moment release occurred between 120 km west and 50 km east of the hypocenter. *Boyd and Nabelek* [1988], who used long-period P and SH waves to invert for the source time-function and seismic moment of the earthquake, also supported this finding. *Engdahl et al.* [1989] showed that seismicity associated with the 1986 earthquake lies between 160 km west and 120 km east of the hypocenter in the middle plane and 0 to 120 km west of the hypocenter in the lower plane. We found the optimal boundary between the Adak high-coupled region and the Atka low-coupled region by testing models with the boundary in different places. We found that any along strike shift in this boundary away from that shown in Figure 2.1 resulted in a worse fit to the data (Figure 2.2b). If the boundary is shifted too far east, the data from the Atka are misfit significantly.

From these findings, we believe our model accurately predicts a significant change in coupling behavior of the middle plane 80 km east of the 1986 hypocenter, while changes in coupling in the other planes occur near the 1986 hypocenter (Figure 2.3). Our recognition of an area of low coupling south of Atka suggests that the 1986 earthquake did not propagate farther east because the creeping region had a low level of shear stress. However, the larger 1957 earthquake began in the western Andreanof region and was capable of propagating through the Atka low coupling region before

rupturing areas farther to the east. The 1957 earthquake may have reached the low coupling region with larger dynamic shear stresses, or if shear stress accumulates very slowly in the Atka region, the 1957 event may have ruptured this area and reduced that shear stress to a very low level. In this second scenario, by 1986 there was not enough shear stress built up to sustain rupture propagation through this region.

We find an arc translation velocity of ~7.8 mm/yr for the Aleutian arc in the Andreanof region (4.9±2 mm/yr arc-parallel). This value is substantially slower than the estimate of *Ekstrom and Engdahl* [1989] (30±10 mm/yr arc-parallel relative to North America), which was based on slip vector azimuths for thrust earthquakes from the Aleutian arc. They used a simple model of slip partitioning in which the relative plate motion between the North American and the Pacific plates is accommodated by slip on the main thrust zone and strike-slip motion on a vertical plane coincident with the volcanic arc. Their analysis of slip vectors also suggested that extension of approximately 30 mm/yr occurs between 160° W and 177° W. *McCaffrey* [1992] also analyzed slip vectors to calculate an arc parallel strain rate for the central Aleutians, and estimated a rate of extension even greater than that calculated by *Ekstrom and Engdahl* [1989]. These findings are in disagreement with our GPS observations, thus indicating either that this type of analysis is not applicable to the central Aleutians or that the structures responsible for slip partitioning are located offshore in the forearc. The velocity we determine for the arc in the Andreanof region is similar to the velocity of Unalaska in the eastern Aleutians (4.7 mm/yr west and 2.7 mm/yr south) [*Mann and*

Freymueller, 2003], indicating that little extension currently exists between the central and eastern Aleutians.

There are currently no identified features inboard of the arc that could be accommodating the motion of the Andreanof region relative to North America. We also note that the Andreanof translation velocity is similar to the velocity measured at St. Paul in the Pribilof Islands 600 km to the northeast. These velocities and other similar velocities in western Alaska and the eastern Aleutians may be related through the existence of clockwise rotating Bering plate as described by *Mackey et al.* [1997].

2.8 Conclusions

Using a fixed model geometry, we have simultaneously inverted for the interseismic coupling in the Andreanof segment of the Aleutian subduction zone and for the velocity of the Aleutian arc in the Andreanof region relative to North America. We find a strong variation in coupling between the west and east ends of this region in agreement with seismicity patterns and moment release for the 1986 Andreanof Islands earthquake. A translation velocity for the arc of 4.1 mm/yr west and 6.7 mm/yr south relative to North America is determined for the Andreanof region. This southwest motion may be related to a clockwise rotating Bering plate.

2.9 References

Boyd, T. M. and J. L. Nabelek (1988), Rupture process of the Andreanof Islands earthquake of May 7, 1986, *Bull. Seis. Soc. Amer.*, *78*(5), 1653-1673.

Ekstrom G. and E. R. Engdahl (1989), Earthquake source parameters and stress distribution in the Adak Island region of the central Aleutian Islands, Alaska, *J. Geophys. Res., 94*, 15,499-15,519.

Engdahl, E. R., S. Billington and C. Kisslinger (1989), Teleseismically recorded seismicity before and after the May 7, 1986, Andreanof Islands, Alaska, earthquake, *J. Geophys. Res., 94*, 15,481-15,498.

Engdahl, E. R. and D. Gubbins (1987), Simultaneous travel time inversion for earthquake location and subduction zone structure in the central Aleutian Islands, *J. Geophys. Res., 92*, 13,855-13,862.

Freymueller, J. T. and J. Beavan (1999), Absence of strain accumulation in the western Shumagin segment of the Alaska subduction zone, *Geophys. Res. Lett., 26*, 3233-3236.

Freymueller, J. T., S. C. Cohen, and H. J. Fletcher (2000), Spatial variations in present-day deformation, Kenai Peninsula, Alaska, and their implications, *J. Geophys. Res.,105*, 8079-8101.

Houston, H. and E. R. Engdahl (1989), A comparison of the spatio-temporal distribution of moment release for the 1986 Andreanof Islands earthquake with relocated seismicity, *Geophys. Res. Lett.*, *16*(12), 1421-1424.

Kisslinger, C. and M. Kikuchi (1997), Aftershocks of the Andreanof Islands earthquake of June 10, 1996, and local seismotectonics, *Geophys. Res. Lett., 24*(15), 1883-1886.

Mackey, K., K. Fujita, L. Gunbina, V. Kovalev, V. Imaev, B. Koz'min, and L. Imeava (1997), Seismicity of the Bering Strait region: Evidence for a Bering block, *Geology*, 25(11), 979-982.

Mann, D. and J. Freymueller (2003), Volcanic and tectonic deformation on Unimak Island in the Aleutian Arc, Alaska, *J. Geophys. Res., 108*(B2), 2108, doi:10.1029/2002JB001925.

McCaffrey, R. (1992), Oblique plate convergence, slip vectors, and forearc deformation, *J. Geophys. Res.,* 97(B6), 8905-8915.

Okada, Y. (1992), Internal deformation due to shear and tensile faults in a half-space, *Bull. Seisl. Soc. Am.,82*(2), 1018-1040.

Savage, J. C. (1983), A dislocation model of strain accumulation and release at a subduction zone, *J. Geophys. Res.*, *88*, 4984-4996.

Sella, G. F., T. H. Dixon, and A. Mao (2002), REVEL; a model for recent plate velocities from space geodesy, *J. Geophys. Res., 107*(B4), doi:10.1029/2000JB000033.

Taber J. J., S. Billings and E. R. Engdahl (1991), Seismicity of the Aleutian Arc, in *Neotectonics of North America*, edited by D. B. Slemmons et al., *Geological Society of America,* Boulder Colorado.

Tanioka, Y. and F. I. Gonzalez (1998), The Aleutian earthquake of June 10, 1996 (M_w 7.9) ruptured parts of both the Andreanof and Delarof segments, *Geophys. Res. Lett.*, *25*(12), 2245-2248.

2.10 Appendices

Appendix 2.1 Andreanof Islands site coordinates and survey history. Numeric values give the approximate number of days surveyed for a given site in a given year.

Network	Station	Latitude	Longitude	1996	1998	1999	2000	2001	2004	2005	Time span (yr)
KANAGA	GATE	51.854	-177.152	0	0	4	0	0	0	6	6.1
	KICM	51.919	-177.196	0	0	2	0	0	0	4	6.1
	KIRH	51.899	-177.093	0	0	2	0	0	0	5	6.1
	ROE2	51.761	-177.124	0	0	10	0	0	0	6	6.1
	MIDK	51.762	-177.235	0	0	9	0	0	0	5	6.1
ADAK	AT18	51.861	-176.641	4	0	1	3	0	0	3	8.8
	BED1	51.878	-176.642	5	0	16	0	0	2	8	8.8
	BETT	51.822	-176.635	0	3	0	0	0	0	4	7
	BR6	51.871	-176.673	2	0	0	0	0	0	6	8.8
	BUGS	51.845	-176.630	3	0	0	3	0	4	3	6.1
	CLUB	51.848	-176.641	0	3	0	3	0	0	4	7.1
	FNGB	51.831	-176.633	0	0	4	0	0	3	3	6.1
	J122	51.878	-176.642	0	0	2	0	0	0	4	6.1
	LORA	51.993	-176.616	0	0	2	0	0	0	5	6.1
	SHTG	51.942	-176.601	0	4	0	4	0	0	3	7.1
	WABM	51.872	-176.705	0	0	4	0	0	0	11	6.2
	WHAL	51.872	-176.707	0	19	15	12	0	0	3	7.1
	ZETP	51.931	-176.556	0	0	3	0	0	0	3	6.1
ATKA	ATKA	52.219	-174.207	0	16	0	11	2	13	0	5.9
	DEC2	52.231	-174.169	0	3	0	3	0	4	0	5.9
	CHUN	52.179	-174.247	0	4	0	3	0	3	0	5.9
	PUPA	52.200	-174.236	0	2	0	3	0	5	0	5.9
	WNDA	52.161	-174.289	0	1	0	2	0	3	0	5.9

Appendix 2.2 Fault plane locations and geometries used for modeling. Positions are listed counter clockwise for all four corners of each fault plane starting with the southeast corner. Dip angle is degrees from horizontal.

Fault planes	Longitude	Latitude	Width (m)	Depth (m)	Dip angle
Adak upper	-174.9533	50.4185	57558	7000	7.99
	-175.0426	50.9277			
	-180.0032	50.4676			
	-179.8624	49.9635			
Adak middle	-173.7458	51.0358	37336	15000	20.38
	-173.7952	51.3487			
	-180.1000	50.7811			
	-180.0096	50.4720			
Adak lower	-175.0811	51.2366	40706	28000	27.82
	-175.1371	51.5582			
	-180.1788	51.1027			
	-180.0888	50.7844			
Adak bottom	-175.1533	51.6618	32449	54000	38.69
	-175.1919	51.8881			
	-180.2702	51.4410			
	-180.2070	51.2170			
Atka upper	-171.8288	50.6730	57558	7000	7.99
	-171.9150	51.1818			
	-175.0731	50.9251			
	-174.9533	50.4185			
Atka middle	-171.9196	51.1787	37336	15000	20.38
	-171.9755	51.4909			
	-173.8140	51.3473			
	-173.7458	51.0358			
Atka lower	-171.9882	51.4918	40706	28000	27.82
	-172.0454	51.8130			
	-175.1598	51.5563			
	-175.0811	51.2366			
Atka bottom	-172.0618	51.9075	32449	54000	38.69
	-172.1009	52.1336			
	-175.2078	51.8869			
	-175.1533	51.6618			

Chapter 3

Evidence for and Implications of a Bering Plate Based on Geodetic Measurements from the Aleutians and Western Alaska[3]

3.1 Abstract

Global Positioning System (GPS) measurements are used to examine the hypothesis of a clockwise rotating Bering plate. Originally proposed based on seismicity patterns and focal mechanisms, the Bering plate encompasses the Bering Sea, western Alaska, and the Aleutian Islands. GPS measurements from the Bering plate's interior (Yukon-Kuskokwim Delta, the Seward Peninsula, and islands in the Bering Sea) show south to southwest motions of 3 to 5 mm/yr. Where GPS data exist, we construct elastic dislocation models to determine the spatial distribution and intensity of locked patches on the Aleutian subduction interface. These models are used to remove interseismic strain from the GPS observation. Using a grid-search inversion procedure, we determine an arc translation velocity for each region of the Aleutians, revealing south and southwest motions of 4 to 9 mm/yr. No active structures are known to accommodate these velocities immediately inboard of the arc, but the arc translation rates are consistent with

[3] Prepared for submission to *Journal of Geophysical Research*, as Cross and Freymueller [2007]

the velocities of sites in the Bering plate's interior. We combine the arc translation rates with measurements from Bering plate's interior sites and estimate the Euler pole for the Bering plate relative to North America. We find this pole to be located at 42.5° N, 121.3° E with an angular speed of 6.0°/my. The clockwise rotation of the Bering plate may cause left lateral faulting in interior Alaska as part of the plate's eastern boundary with the North-American plate. The Bering plate's interaction with southcentral Alaska may be responsible for the decreased slip-rate on the Denali fault west of the Denali massif, and for contraction across the Alaska Range. Using the newly defined Bering plate motion we analyze slip partitioning along the Aleutian arc based on both GPS measurements and slip azimuths of thrust earthquakes. We find a systematic discrepancy between plate convergence direction and slip azimuths and find that slip partitioning in the back-arc only develops west of Amchitka Pass whereas slip partitioning in the forearc is present throughout the arc.

3.2 Introduction

The Bering Sea is bordered by Alaska to the east, by Russia to the west, and by the Aleutian Islands to the south. This body of water covers a great expanse of continental crust that extends hundred of kilometers west from the coast of western Alaska. The geology of this submerged land is poorly understood, with only a few islands to offer clues regarding ages and terrane affinities. Some knowledge has been obtained from geophysical surveys, so as to recognize the existence of extensive young volcanism and sedimentary deposition [*Cooper et al.,* 1992]. Without a sufficient

knowledge of terranes and their structural relations, geologic observations provide virtually no information about young tectonics of this continental lithosphere, an area nearly the size of Alaska itself. West of Alaska's Bering Sea islands lies a passive margin connecting the submerged continental crust to the oceanic crust underlying the Aleutian Basin. The Bering Sea floor is seismically very quiet with only a few events and no well defined spatial patterns. Yet, studies of seismicity from the Bering plate's margins led to the first theories regarding the tectonics of the Bering Sea region.

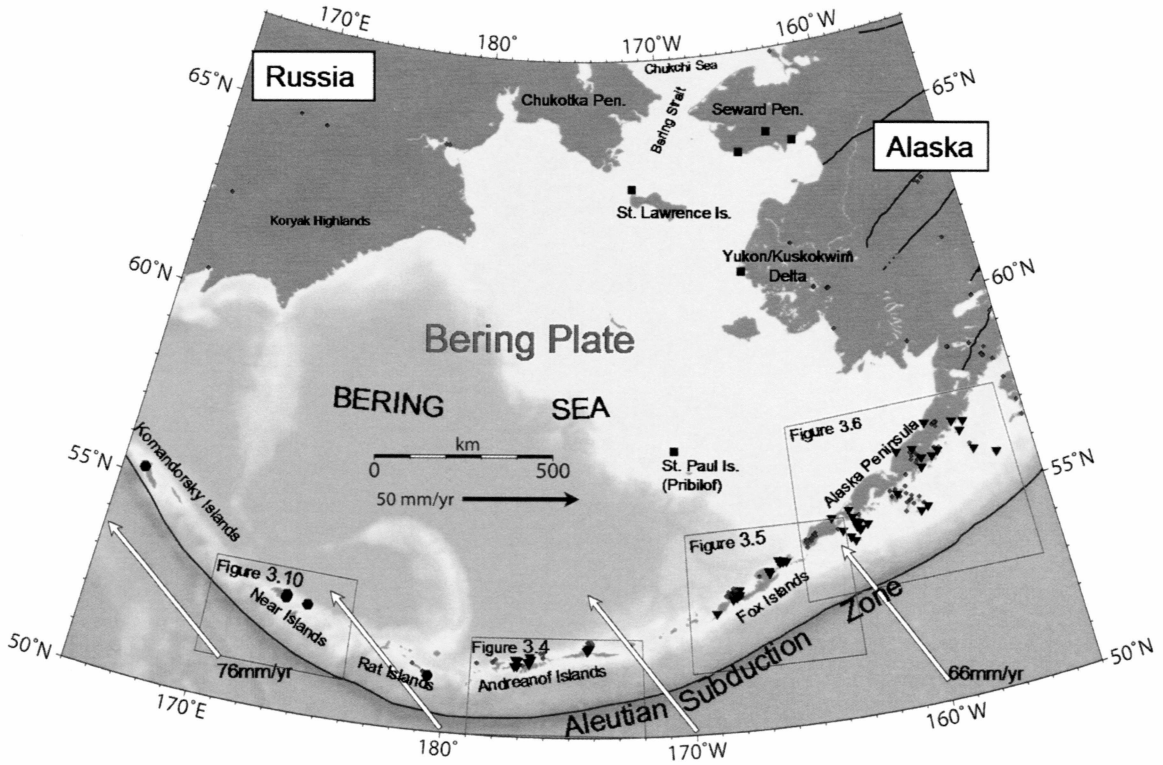

Figure 3.1 Overview map of the study area. Map shows important geographic features and the locations of other figures in this paper. GPS survey locations are shown as follows: squares are sites from the Bering plate interior, inverted triangles are sites used in geodetic models for the Aleutians, hexagons are sites in the far western Aleutians, all other sites are shown as small diamonds. The white vectors show the velocity of the Pacific plate relative to stable North America.

The Seward Peninsula is located in the central area of the western coast of Alaska and is surrounded by the Chukchi Sea to the north, the Bering Strait to the west, and the Bering Sea to the south. The western end of the Seward Peninsula is less than 100 km from the Chukotka Peninsula, Russia (Figure 3.1). The Seward Peninsula is considered part of the North American tectonic plate; however, it is one of the most seismically

active areas of Alaska outside of a recognized plate boundary [*Fujita et al.,* 2002]. Earthquakes here are primarily tensional and a breadth of geologic and geophysical data suggests the onset of continental rifting [e.g. *Turner and Swanson,* 1981*; Dumitru et al.,* 1995*; Page et al.,* 1991]. The original evidence for young to active extension on the Seward Peninsula came from geologic mapping and the recognition of young normal faults with 4 to 10 meters of Holocene offset [*Hudson and Plafker,* 1978]. *Turner and Swanson* [1981] proposed that these faults are part of an incipient rift through the Seward Peninsula on the basis of their association with geothermal anomalies and young basalt flow deposits.

Clockwise rotation of a Bering plate could provide a mechanism to drive extension on the Seward Peninsula. A Bering plate has been proposed ever since the earliest plate tectonic models based almost entirely on seismicity. *Minster et al,* [1974] proposed a Bering plate to explain misfit of earthquake slip vectors along the Aleutian arc. *Lander et al.* [1996] proposed a "Beringia plate" to explain the seismicity of the Koryak Highlands, Russia. *Mackey et al.* [1997] presented a more convincing argument for a Bering plate based primarily on newly compiled Russian and US seismological data. The location of seismic events around the Bering Sea roughly defines the extent of the Bering plate. A broad area of deformation extends across the Seward Peninsula to the Chukotka Peninsula and from there southwest through the Koryak Highlands to Kamchatka. Focal mechanisms indicate normal faulting in the Seward Peninsula that transitions into right-lateral strike-slip faulting to the west. The Koryak Highlands are

dominated by thrust events that may define the western boundary of the Bering plate. The southern boundary is defined as the Aleutian subduction zone [*Mackey et al.,* 1997].

Geodetic measurements using GPS provide a way to quantitatively analyze the Bering plate hypothesis, but not without complications. With the exception of the Bering plate margins and a few remote islands, the Bering plate is sub-aqueous, thus geodetic observations are concentrated on the edges of the plate where plate interactions result in strains outside of the plate's rigid body motion. These strains must be removed from the GPS observations by modeling to properly determine the plate's velocity at a given location. This is especially true for the Aleutian arc, an area that contains the highest number of observations anywhere on the Bering plate (Figure 3.1).

Previous geodetic studies on the lower Alaska Peninsula, where Pacific–North America convergence direction is almost entirely trench normal, recorded velocities of ~4 mm/yr to the southwest [*Freymueller and Beavan*, 1999; *Mann and Freymueller*, 2003]. These studies found little indication of strain associated with subduction, and therefore interpreted the velocities as a southwestward translation of those regions relative to stable North America. *Cross and Freymueller* [2007] used elastic dislocation modeling to remove interseismic strain from GPS measurements in the Andreanof region of the Aleutian arc. They were able to determine the spatial pattern of coupling on the subduction interface while also finding that the Andreanof region is translating southwest relative to North America.

In this study, we apply the same technique to other regions of the Aleutians and Alaska Peninsula primarily to determine the motion of the arc relative to North America.

GPS geodetic measurements have also been recorded in western Alaska, and on the Bering Sea Islands of St. Paul (Pribilof Islands) and St. Lawrence (Figure 3.1). We combine these measurements with modeled arc translation rates from the Aleutians to quantitatively evaluate the Bering plate hypothesis, and investigate its bounding regions.

3.3 Modeling Aleutian Arc Geodetic Observations

3.3.1 Methodology

Strain accumulation at a subduction boundary is modeled using elastic dislocation theory following the approach of *Savage* [1983] and the computational methods of *Okada* [1992]. The earth is represented by a uniform elastic half-space and the plate interface by one or more rectangular planar faults, and the strain accumulation rate is assumed to be constant through the interseismic period. The interseismic deformation rate is computed from the superposition of steady state subduction along the entire plate interface, and steady normal slip (back slip) in the main thrust zone at the plate convergence rate, resulting in a plate interface that has a locked main thrust zone and is slipping freely above and below this zone (Figure 3.2) [*Savage,* 1983]. Appropriate strike-slip and dip-slip components are determined by the convergence direction of the subducting plate and the strike of the trench. Because the Aleutian arc is moving relative to North America, the convergence velocity is the Pacific plate velocity minus the North American plate velocity minus the velocity of the Aleutian Arc relative to stable North America.

Like many past authors, we extend the method of *Savage* [1983] by allowing the main thrust zone to be either fully locked or partially creeping, with the slip deficit on the

interface parameterized by a coupling coefficient. The coupling coefficient is one minus the slip between the two plates expressed in terms of a unit plate convergence rate. For example, if there is no slip the coupling coefficient is one, and if the slip between the two plates is equal to the rate of plate convergence, the coupling coefficient will be zero. The coupling coefficient can represent the percentage of the total interface that is locked.

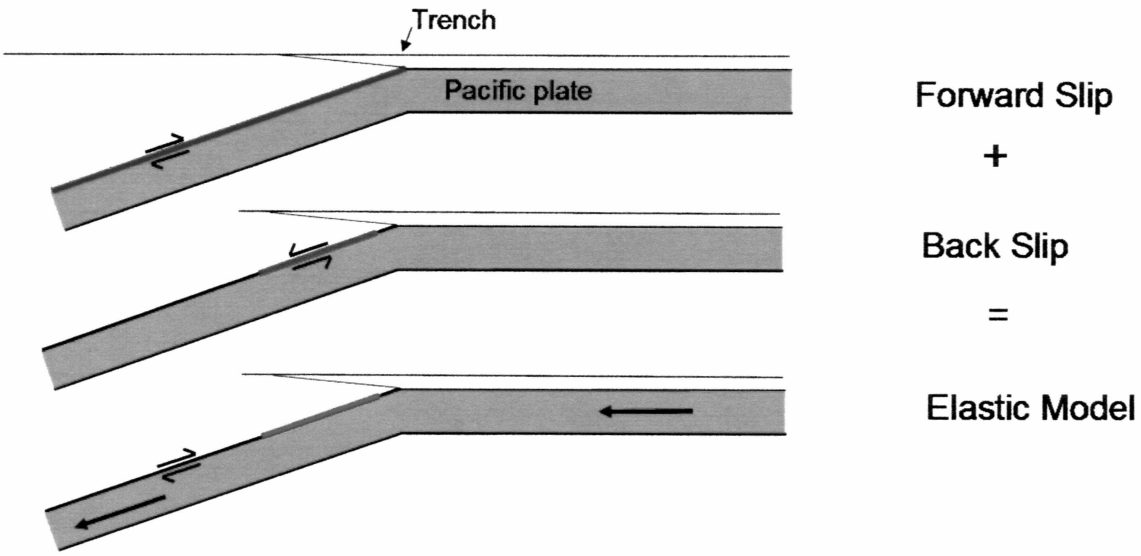

Figure 3.2 Two dimensional dislocation model. The elastic dislocation model is based on the methods of *Savage* [1983] and is composed of two parts: forward slip and back slip which are superimposed to give a dislocation that is locked in the main thrust zone and slipping freely above and below this zone. *Savage* [1983] assumed that steady forward slip does not produce deformation, so the observed deformation is due entirely to the back slip component.

All measurements made at sites near a subduction zone are composed of two components, a component of interseismic strain caused by the subducting plate and coupling on the main thrust zone, and a component of rigid body translation that represents the long term motions of the sites (Figure 3.3). We are interested in determining the rigid body translation or "arc translation velocity" as this motion may be representative of the Bering plate motion. To isolate the arc translation velocity we must model the interseismic strain with an elastic dislocation model and remove this component from our measurements.

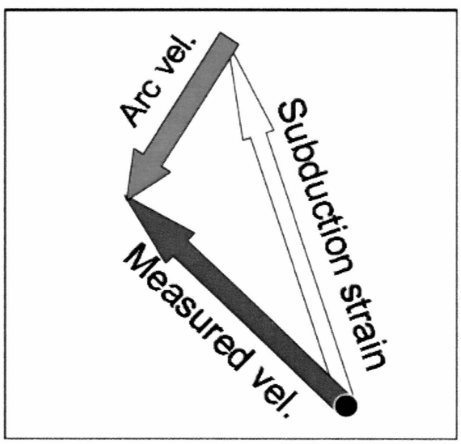

Figure 3.3 Diagram of vector components. The arc translation velocity (Arc vel.) may represent the motion of the Bering plate, but to determine this velocity we must remove the component of subduction strain from the measurements.

We use a grid-search inversion procedure to solve for both the translation velocity of the arc and the coupling on the fault planes. The first step is to modify our data by subtracting from it an arc translation velocity from a grid of candidate arc velocities. If

we have selected the correct arc velocity this procedure isolates the component of our measurement that is caused entirely by interseismic strain and thus can be modeled using the elastic dislocation model. Using a fixed fault plane geometry, we calculated the 3D surface displacements at each station assuming 100% coupling on all fault planes to obtain the Green's functions needed for the inversion. We invert for the coupling coefficients (m) using a MATLAB script "lsqlin", which solves for m with linear least squares technique with inequality constraints. Using the coupling coefficients we can now compare modeled velocities to our measured velocities and calculated a chi squared value. This inversion procedure is executed for each candidate arc velocity and the chi squared values are compared to reveal the best arc translation velocity and its 95% confidence region. The fault plane coupling coefficients associated with the best arc translation velocity represent the subduction interface behavior.

3.3.2 Andreanof Islands Region

Cross and Freymueller [2007] used GPS measurements in the first quantitative study of plate coupling on the Andreanof segment, Aleutian subduction zone. A dislocation model was constructed to estimate the velocity of the arc and fault plane coupling coefficients in the Andreanof region (Figure 3.4). The fault plate geometry used was based on seismic studies by *Engdahl et al.* [1989], *Ekstrom and Engdahl* [1989] and by *Engdahl and Gubbins* [1987], and the best-fitting model had an arc translation velocity of 4.1 mm/yr west and 6.7 mm/yr south. The results of *Cross and Freymueller* [2007] revealed little to no coupling in Atka (eastern Andreanof Islands) and very strong

coupling in the Adak region (western Andreanof Islands); this result is consistent with the moment release distribution and seismicity patterns of previous major earthquakes (Figure 3.4, [*Ekstrom and Engdahl,* 1989; *Houston and Engdahl,* 1989; *Boyd and Nabelek,* 1988]).

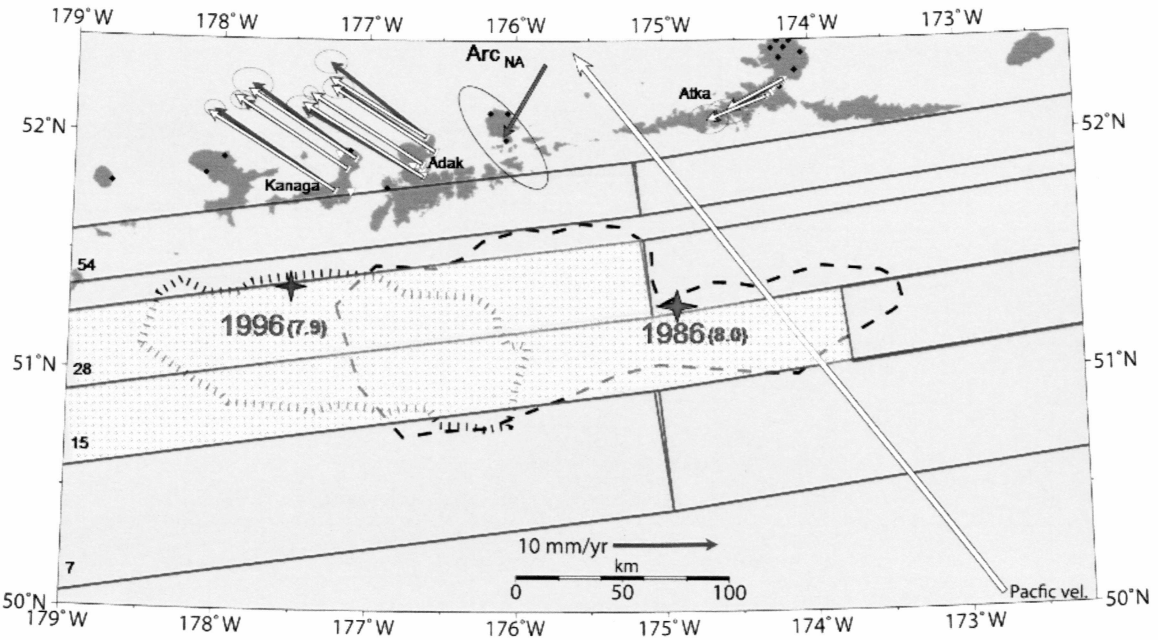

Figure 3.4 Summary of modeling results for the Andreanof region, modified from *Cross and Freymueller* [2007]. Measured (blue) and modeled (white) velocities are shown relative to stable North America for sites located in the Andreanof region of the central Aleutians. The red arrow ($Arc_{N.A}$) is the best-fit arc translation velocity of the Andreanof region. Ellipses represent 95% confidence limits. The long white arrow is the velocity of the Pacific plate. Pink stippled area designates fault plane regions with high coupling. Dotted and dashed outlines represent the rupture areas for the 1996 and 1986 earthquakes respectively. Epicenters are shown as stars. GPS sites are shown as inverted triangles if they are used in this study and other GPS sites are indicated by black dots. Depths in km to the top of each fault plane are listed at the far west edge.

3.4 Data and Model Results

3.4.1 GPS Data

Velocity estimates are primarily obtained from episodic or survey mode GPS measurements (SGPS) of survey benchmarks. A few velocities are based on continually operating GPS sites (CGPS). CGPS sites provide more accurate velocities in a shorter amount of time but are expensive to install and maintain, especially in remote parts of Alaska. Precise velocities from many new CGPS sites will be available in the next few years as a result of the National Science Foundation's Earth Scope program.

Many GPS sites throughout the Aleutians Islands have been surveyed as part of an effort to record volcanic deformation. For most of these sites there is not enough information to confidently remove the volcanic signal; therefore, we only used sites that do not show signs of volcanic deformation.

Western Alaska is an enormous area, and geodetic measurements from this area are exceedingly sparse. With the use of rural village airport survey data and quality repeat geodetic surveys in the summers of 2005 and 2006, we have obtained velocity estimates for a few locations in western Alaska and the Seward Peninsula. In the Yukon/Kuskokwim Delta, we have two velocities, HOOP in Hooper Bay and BETC in Bethel. On the Seward Peninsula, we have three velocities, OMEA in Nome, MELS in Council, and ELIB in Elim. Two other important and surprisingly well surveyed sites are GAMB on St. Lawrence Island and SPSW on St. Paul Island. Some of these velocities are determined based on more than one site. For instance, in Nome there are at least five sites within a few kilometers of each other. There is no reason to believe that these sites

should have different velocities, and where proper survey ties exist, we combine the data to obtain the best velocity possible for Nome.

We used the GIPSY/OASIS II software version GOA4 to obtain daily coordinate and covariance estimates of our stations and regionally distributed stations in the ITRF2000 reference frame [e.g., *Freymueller et al.,* 2000]. We estimated site velocities in ITRF2000, and then converted to velocities relative to the North America plate by subtracting the motion of North America in ITRF2000. The North America plate motion is based on velocities from 124 continuous GPS sites that have been identified to be free of tectonic and isostatic motions [*Sella et al.,* 2007]. This realization of the North American plate motion is an improvement over the REVEL2000 model of *Sella et al.* [2002] that was used in previous studies. This new realization of the North America reference frame changes the measured velocities. For example, the site SPSW on St. Paul, which we propose to lie on the Bering plate interior, shifts from its previous velocity by 2.4 mm/yr east and 0.5 mm/yr south. The difference between the two estimates of the motion of the North American plate arises from changes in the selection of sites that are used to define the plate's motion, and from a change in the global reference frame. REVEL2000 used the ITRF97 reference frame and differences between ITRF97 and ITRF2000 appear to be on the order of 1 to 2 mm/yr. Because our velocities are determined in ITRF2000, it is more consistent to use the *Sella et al.* [2007] realization of a North America reference frame. The velocities and uncertainties relative to stable North America are listed in Appendix 3.1.

3.4.2 Andreanof Islands

Using the new reference frame realization we reanalyze the Andreanof Island region. We use the same eight fault plane model as *Cross and Freymueller* [2007] (Figure 3.4 and 3.5). The fault geometry parameters are listed in Appendix 3.2. We find the optimal boundary between the Adak and Atka "middle" plane by testing models with the boundary in different locations along strike. The boundary condition $0 \leq m \leq 1$ is applied to all fault planes except the bottom plane on the Adak side where m is allowed to range between -1 and 1. This negative coupling coefficient condition allows for afterslip and/or viscous relaxation that could be present below the main thrust zone due to the 1986 or 1996 earthquakes.

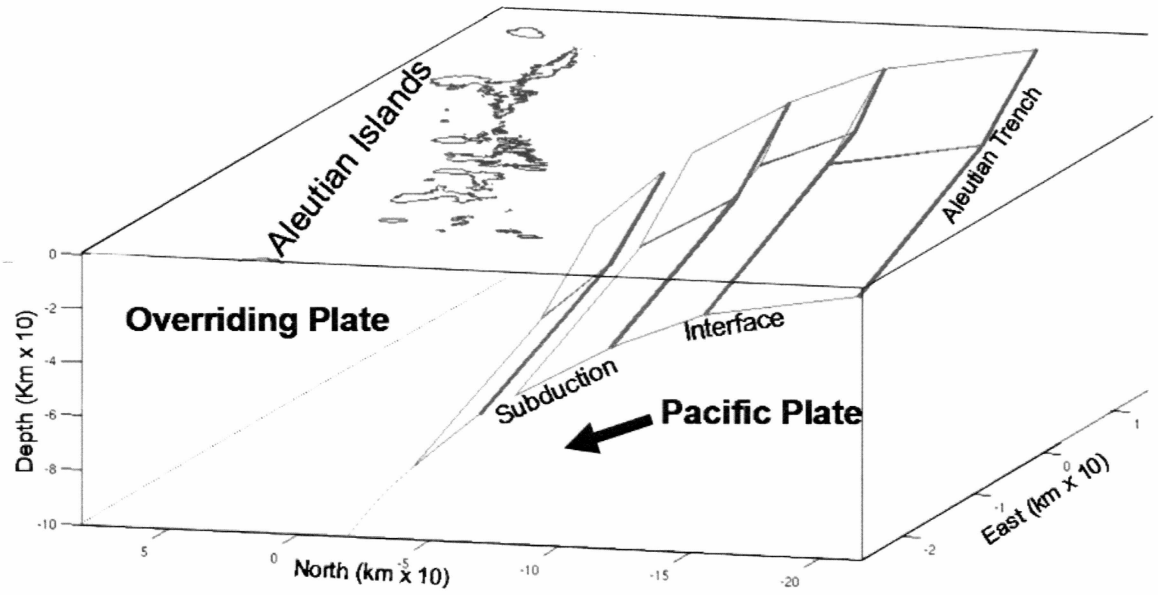

Figure 3.5 3D fault dislocation model for the Andreanof region. The subduction interface is represented by eight fault planes that increase in depth and dip away from the trench axis. The coupling on each of these fault planes is calculated using the grid-search inversion procedure described above. Axes for this figure are in a local coordinate system centered at site BED1 on Adak (See Appendix 3.1).

Because the convergence direction depends on the arc velocity relative to North America (which is unknown), the inverse model is non-linear and we solve for the arc velocity and plate-coupling coefficients using a gridded search-inversion procedure described above. We find an arc translation velocity of 0.4 mm/yr west and 7.9 mm/yr south (Figure 3.6). The coupling coefficients for each fault plane are shown in Figure 3.7. Although there is a significant change in the arc velocity from the previous analysis by *Cross and Freymueller* [2007], we find there is still good agreement between the areas of high coupling and the rupture zones of past major earthquakes. One fault plane, the Atka upper plane, has a drastic coupling coefficient change from 0% in the previous

analysis to 79% in the new analysis. This change is not significant though because the uncertainty range for the upper planes is 0 to 100% (Appendix 3.2).

The change in the arc translation velocity highlights the importance of having a well-defined reference system as the same data set was used in the previous and current study, and the only difference in the new study was the way the motion of the North American plate was defined. Compared to the old arc velocity for the Andreanof region, the new arc velocity is 3.7 mm/yr more to the east and 1.2 mm/yr more to the south. These changes are larger than the changes caused by the reference frame alone, which are 2.4 mm/yr east and 0.1 mm/yr south for the Andreanof region.

We determined the 95% confidence limits for each coupling coefficient by allowing the arc translation velocity to vary within its 95% confidence region and by fixing the other coupling coefficients at their best value while varying one at a time and comparing the minimum chi squared values. The upper planes are the most poorly determined and have an uncertainty that is greater than their physical range of values. In other words, we cannot confidently say anything about the coupling on the upper planes except that coupling on these planes does not significantly affect the model results at the 95% confidence level. In general, the planes in the Adak region are better determined than the Atka region planes; this is due to a greater range of trench normal measurements in the Adak region. The best values for the fault plane coupling coefficients and their 95% confidence ranges are listed in Appendix 3.2.

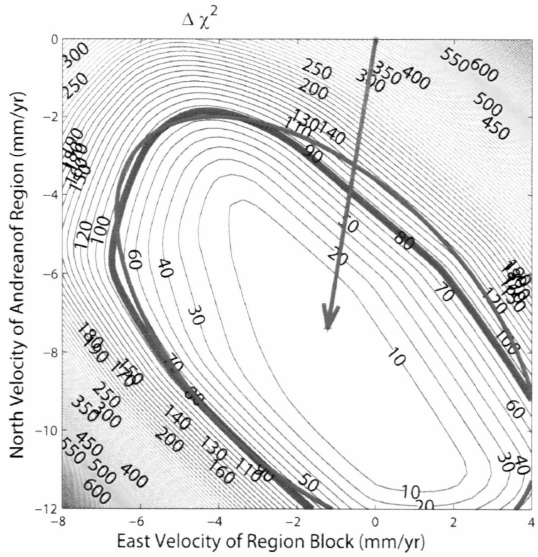

Figure 3.6 $\Delta\chi^2$ contour plot vs. arc velocity for Andreanof region. $\Delta\chi^2$ is contoured based on minimum values at a range of east and north arc translation velocities. Contour lines are equally spaced at intervals of 10 above the minimum χ^2 value. The best arc velocity is 0.4 mm/yr west, and 7.9 mm/yr south. The 95 % confidence region is outlined by the thick blue line, red ellipse is the best fit ellipse to the 95% confidence region.

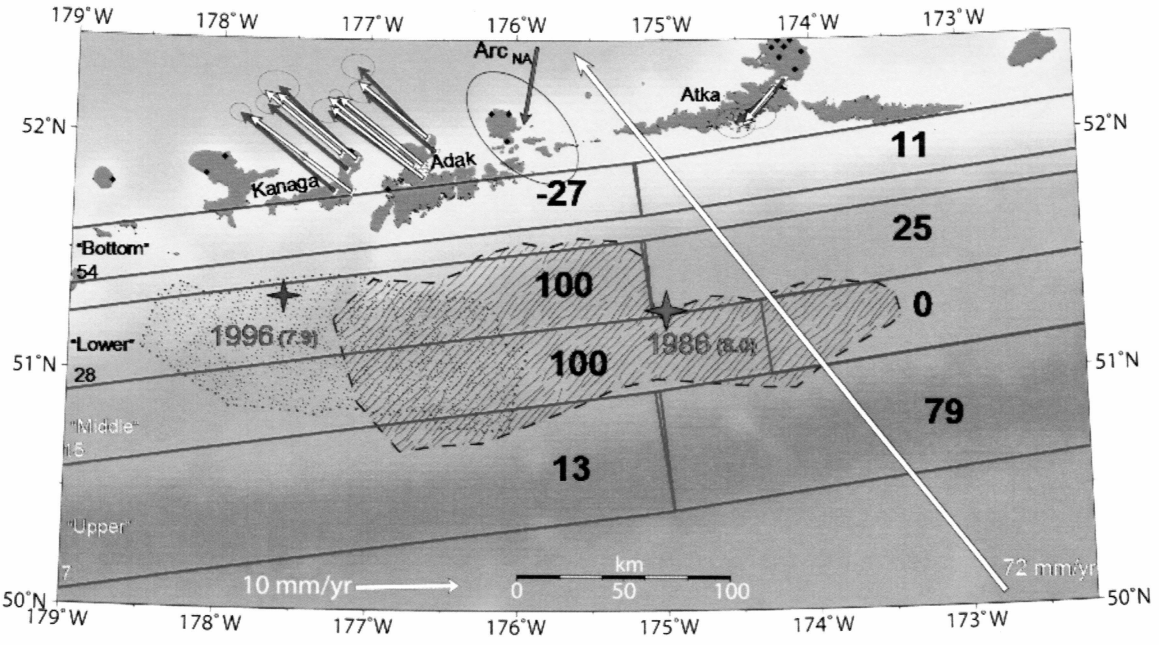

Figure 3.7 New dislocation modeling results for Andreanof Islands region. Measured velocities are shown in blue and modeled velocities are shown as white vectors. All velocities are relative to stable North America (*Sella et al.* [2007] realization). Bold numbers denote the percent of unit coupling for the associated fault plane (see Appendix 3.2 for uncertainties). The error ellipse for the arc translation velocity is based on best-fit ellipse to the 95% confidence region shown in Figure 3.6. The component of the arc translation velocity in the direction of plate convergence is less certain because of tradeoffs between the arc velocity and plate coupling. Epicenters are shown as stars. The depth to the top of each set of fault planes in kilometers is shown at the west end; the top of the upper fault planes corresponds to the trench location. GPS sites are shown as inverted triangles if they are used in this study and other GPS sites are indicated by black dots.

3.4.3 Fox Islands

Data from the Fox Islands region includes sites on Umnak, Unalaska, and Akutan Islands (Figure 3.8). All of these islands are home to large active volcanoes, yet on each island, there is at least one site located far enough away from volcanic activity to avoid recording volcanic deformation. On Umnak Island, the vast majority of GPS measurements have been established to record deformation associated with Okmok Caldera on the northeast end of the island. A few sites on the southern shoreline of Okmok have linear time series that do not appear to be affected by episodic volcanic intrusions. However, a 3 mm/yr discrepancy in the north velocity exists between these sites on Umnak Island and the site UNAL 10 km to the southeast on the southwest tip of Unalaska Island. This difference is not resolvable with any realistic fault model and we ultimately chose not to include the sites closer to Okmok Caldera. Changing the selection of data in this case has drastic effects on our results and leads us to conclude that we cannot be very confident in our final model for this region.

The site ROWD on the western end of Umnak is the only site between Okmok and the Andreanof Islands 300 km to the west, and thus provides the only geodetic clues as to the subduction zone behavior in this region. On Unalaska Island, all of the sites are located near the town of Dutch Harbor; there is remarkable self-similarity among the numerous sites as they are located no more than 8 km apart. On Akutan Island, all but four of the sites are affected by volcanic deformation associated with Akutan Volcano. Sites on Akutan show velocities very similar to Unalaska (Appendix 3.1, Figure 3.8).

In the Andreanof region, previous seismic studies by *Engdahl et al.* [1989] and *Ekstrom and Engdahl* [1989] used data from local and teleseismic stations to reveal the shape of the subduction zone. To construct the fault model in the Fox Islands region, we use the location of the trench, the volcanic axis, focal mechanisms from large thrust events, and the location of smaller earthquakes to constrain the fault geometry.

We use a five fault plane model as shown in Figure 3.8. The fault geometry parameters are listed in Appendix 3.2. Because there is up to a 7.4 mm/yr difference in the trench normal displacements measured along strike, we assume coupling varies along strike and subdivide the fault plane model to accommodate this behavior. We optimize the boundary between fault planes 2 and 3 by testing models with the boundary at different locations along strike and finding the model with the best fit to the data. Because there is a limited spatial distribution of data, we refrain from further complicating the geometry and assume that planes 1, 4, and 5 have uniform coupling along strike.

In the Fox Islands region, the distance between the trench and the volcanic arc increases approximately 30 km from west to east. Because the dislocation program only accepts rectangular dislocations, we replicated this geometry by changing the strike of the planes for different depths and by having a shallower dip and greater width for plane 2 than plane 3. This results in imperfect boundaries between fault planes, but we make an effort to minimize gaps and overlapping regions (Figure 3.8). The remaining gaps are small enough to have minimal impact on our model calculations. We execute the inversion for the model parameters in the manner described in Section 3.3.1, with the

coupling on the fault planes constrained to be between 0 and 100% of the plate convergence for all fault planes.

The results of the Fox Islands region modeling are displayed in Figure 3.8. Coupling is high in the shallow planes and very low in the two deepest planes. Coupling is higher in plane 3 than plane 2, which allows for a better fit to sites ROWD and UNAL. We find an arc translation velocity of 3.6 mm/yr east and 14.3 mm/yr south (14.6 mm/yr arc normal, 2.4 mm/yr arc parallel). This arc translation velocity is well determined in the arc parallel direction but has a very elongated 95% confidence ellipse in the plate convergence direction. This uncertainty results from tradeoff between coupling on the fault planes and arc translation in the direction of plate convergence. Arc translation in this direction would be better constrained if we had more sites with a greater range of trench normal distances. Uncertainties for the coupling coefficients are listed in Appendix 3.2.

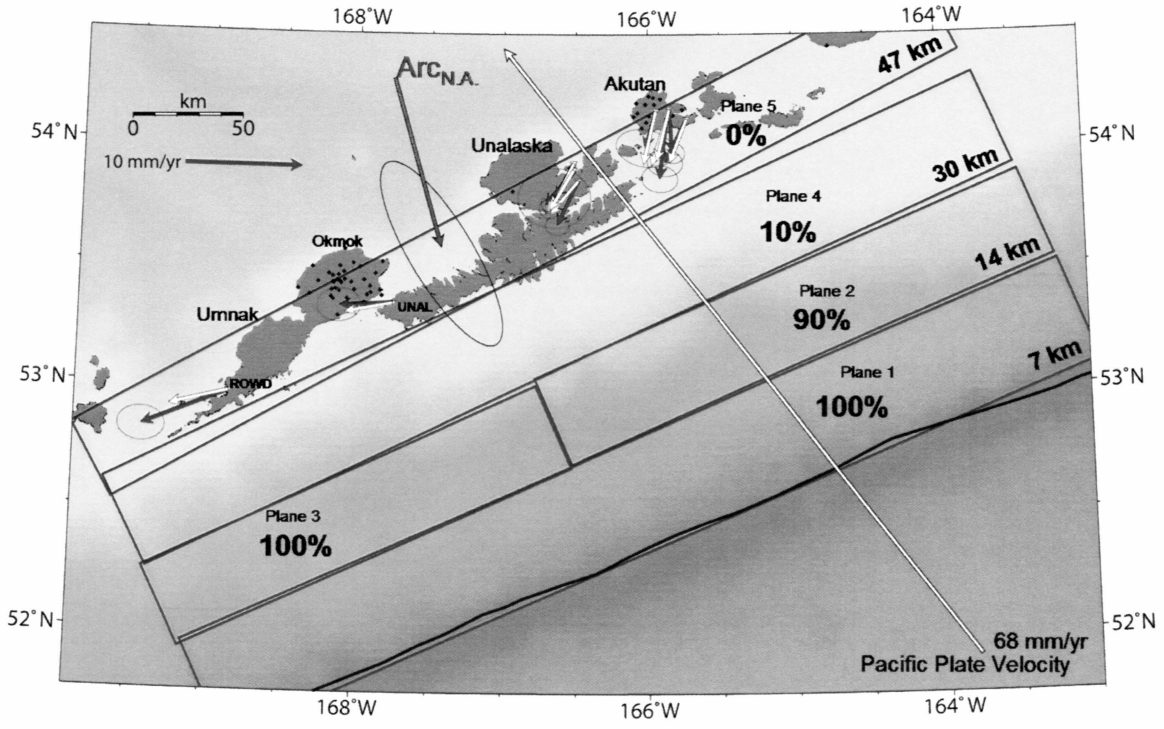

Figure 3.8 Geodetic modeling results for the Fox Islands region. Color-coding is the same as Figure 3.7, and all velocities are relative to North America. Note the higher coupling in plane 3 because of sites ROWD and UNAL.

3.4.4 Alaska Peninsula

The Alaska Peninsula region includes data from Chirikof Island (west of Kodiak) at 155° W to Sanak Island at 163° W, an along strike distance of approximately 500 km (Figure 3.9). This region of the Aleutian arc has the greatest trench normal range of data of any region and many of these sites have well determined velocities (Appendix 3.1). A geodetic study by *Fletcher et al.* [2001] used data from the Chirikof Island region to estimate an interseismic coupling value of 80%. With an improved data set, *Fournier*

and Freymueller [2007] used the method of simulated annealing to estimate the optimal fault model for this region. To avoid over-parameterization the authors chose to use only four fault planes to represent the subduction interface. *Fournier and Freymueller* [2007] assumed a fixed arc translation velocity and found the coupling on the four fault planes to be 90%, 70%, 30% and 0% from east to west. This finding is in agreement with seismicity patterns. Specifically, the 1938 M_w 8.3 ruptured the eastern two planes, whereas the western region is dominated by creep and has seen less moment release over the last 100 years. This western region is often referred to as the Shumagin seismic gap.

We use the same four fault planes but re-estimate plate coupling and the arc velocity using the grid-search inversion procedure described in Section 3.3.1 with an improved North American reference frame. The estimated coupling coefficients and arc translation velocity are shown in Figure 3.9. We find an arc translation velocity of 2.1 mm/yr west and 3.4 mm/yr south (1.9 mm/yr arc normal and 3.6 mm/yr arc parallel, 4.0 mm/yr at 211°). This is similar to the fixed arc velocity of 5.3 mm/yr at 241° used by *Fournier and Freymueller* [2007] but shifted by the amount expected when using the new North America reference frame [*Sella et al.,* 2007] vs. the older REVEL reference frame [*Sella et al.,* 2002]. The coupling coefficients illustrate that the subduction interface is nearly fully locked (90%) at the Semidi Islands, decreasing to about 30% locked at the Shumagin Islands, and freely slipping to the west of the Shumagin Islands near Sanak Island. Thus, the measurements recorded in the western network where very little strain is observed are almost entirely the result of the southwestward translation of the arc.

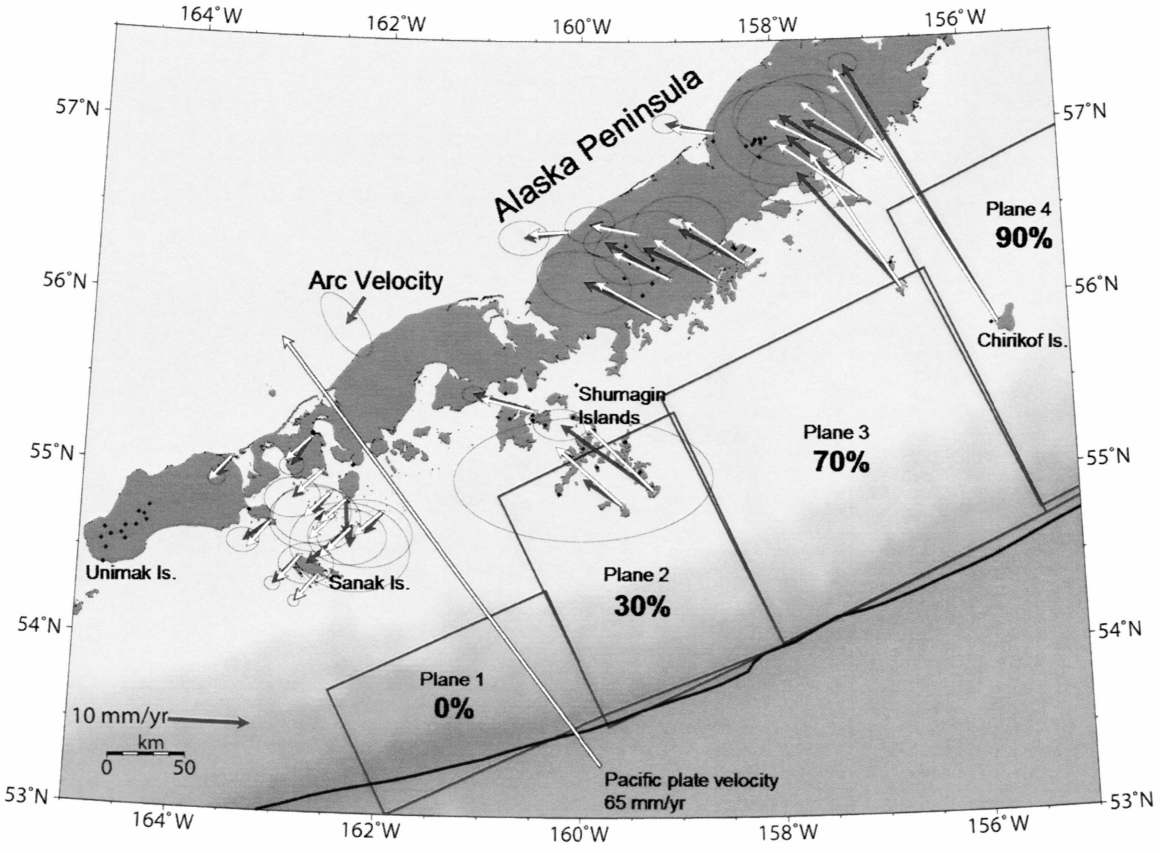

Figure 3.9 Geodetic modeling results for the Alaska Peninsula. Color-coding is the same as Figure 3.7 and all velocities are relative to North America. Measured velocities in the lower or western Alaska Peninsula are primarily explained by the arc translation velocity relative to North America shown by the red arrow. The very low coupling coefficients for this region indicate the subduction zone interface is slipping freely.

Table 3.1 Calculated arc translation velocities in mm/yr relative to North America.

Region	East	North	E_σ	N_σ	Correlation	Arc //	Arc ⊥
Andreanof	-1.14	-7.59	1.62	1.81	-6.77	2.14	7.37
Fox	3.63	-14.33	1.22	1.86	-8.60	2.45	14.58
AK Pen.	-2.14	-3.43	0.75	0.93	-6.70	3.56	1.93

3.4.5 Western Alaska and Bering Sea Island Data

The data from western Alaska and the Bering Sea islands (Figure 3.10) show southward velocities of 3 to 5 mm/yr (Appendix 3.1). We only consider sites to move as part of the Bering plate stable interior if they pass the following requirements. First, sites must lie far enough away from the subduction zone to not record postseismic deformation from the 1964 Great Alaska Earthquake or active interseismic strain. This eliminates sites such as LIME and MGRA or any sites within a few hundred km of the subduction zone. We have developed models for sites that are only affected by interseismic strain as shown in the previous sections, but we cannot remove postseismic deformation at this time as accurate models do not yet exist. Sites must also not be affected by the 2002 Denali Fault earthquake. This eliminates any sites in interior Alaska. There are a few pre-Denali earthquake velocities for interior Alaska but these measurements are either poorly determined or show velocities clearly different from western Alaska (see Section 3.7.1). We also exclude the site BETC in Bethel, because an F-test reveals that this site has a motion significantly different from other Bering plate interior sites at the 90% confidence level. BETC might also be subject to 1964 postseismic deformation, but with only two surveys of this site, it is difficult to know why it does not agree. Removing BETC does not significantly affect the Euler pole for the Bering plate (Section 3.5).

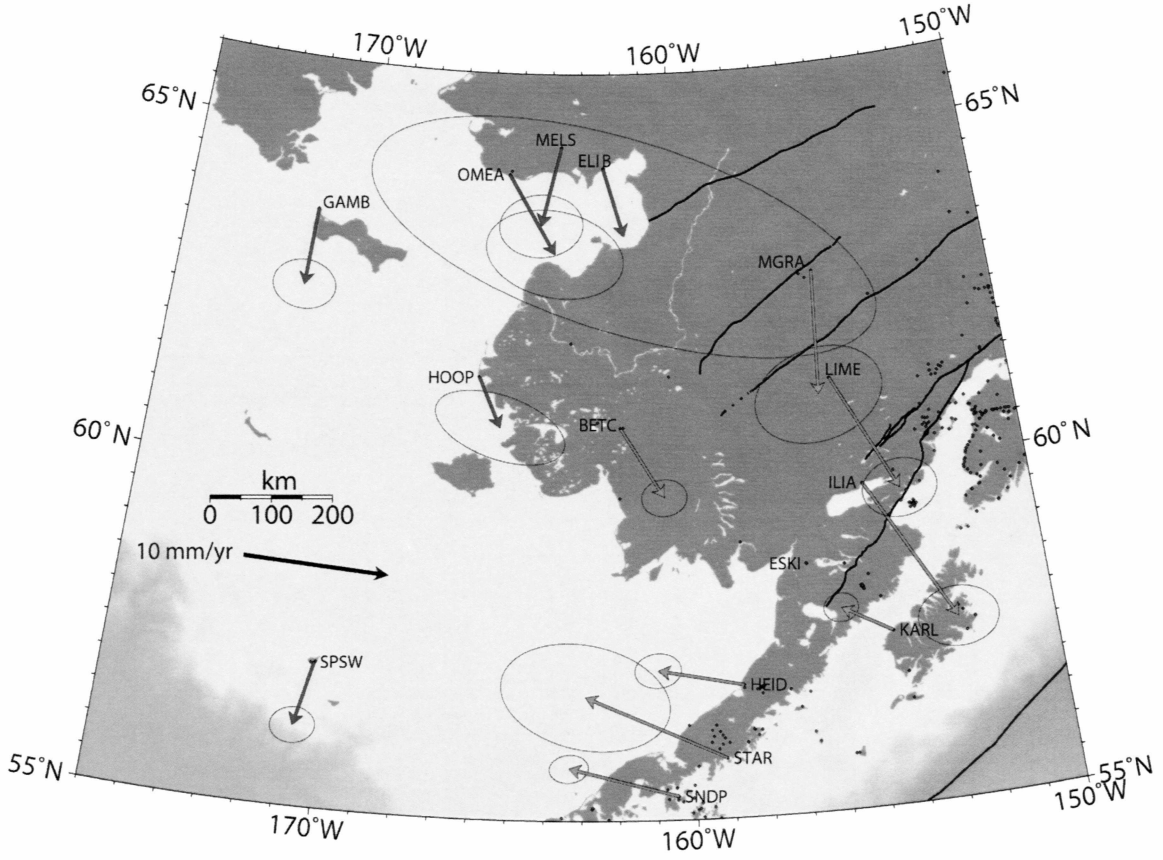

Figure 3.10 Map showing velocities of Bering plate interior sites. Measured velocities of sites in Western Alaska and the Bering Sea islands relative to stable North America. Sites shown in blue are considered to move as part of the Bering plate, grey vectors are sites that have a velocity significantly different from that of the Bering plate.

There is no obvious active structure dividing the Bering plate interior from the Aleutians. The measurements from this region are similar to the arc translation velocities calculated for the Aleutians, thus indicating that the Aleutian arc and western Alaska are probably moving as part of the same plate but not as part of North America. To test this hypothesis we combine all the data from the Aleutians, western Alaska, and the Bering Sea islands to estimate the angular velocity of the Bering plate relative to North America.

3.5 Euler Pole Inversion

Euler's theorem, when applied to plate tectonics, states that the surface velocities of any plate or pair of plates is described by the orientation of a pole or axis with its origin at the center of the earth and by its angular speed ω. This linear relation allows us to use measurements from the Bering plate interior to directly invert for an Euler pole using a linear least squares approach. The cross product describes the mathematical relation between each site's velocity and the Euler pole (Equation 3.5.1).

$$v = \omega \times r = \begin{bmatrix} 0 & r_z & -r_y \\ -r_z & 0 & r_x \\ r_y & -r_x & 0 \end{bmatrix} \begin{bmatrix} \omega_x \\ \omega_y \\ \omega_z \end{bmatrix} = Gm \tag{3.5.1}$$

$$m = (G^T \cdot \mathrm{cov}^{-1} \cdot G)^{-1} \cdot (G \cdot \mathrm{cov}^{-1} \cdot V) \tag{3.5.2}$$

In vector form, ω, r, and v are all three-component vectors in an earth centered Cartesian coordinate system (xyz). A site's velocity is v and the distance to the Euler pole is described by the vector r. The Euler pole can be described by an Earth centered angular velocity vector (ω) that points in the direction of the Euler pole, and the length of ω is the angular speed. In matrix form, we invert for the three components of the Euler pole (m) using Equation 3.5.2. In this equation, G is the Green's functions that map the unit velocity from each site to the Euler pole, V is the measured velocities of all the sites in xyz, and cov is the full covariance matrix for the data.

In addition to the Bering plate interior sites, we have used the arc translation velocities calculated for the central and eastern Aleutians and Alaska Peninsula to augment this inversion. The translation velocities are based on many measurements, but

each is given the same weight as one interior site, as they are representative of only one location. The one-sigma uncertainty of the data is used in the inversion to calculate the 95% confidence error ellipse for the Euler pole locations (Figure 3.11).

We use a F-test to analyze the significance of the Bering plate motion. The F-test compares the misfit of two models, where the fist model represents a null hypothesis and a second model includes additional adjustable parameters. Because the misfit to the data is expected to decrease when there are more adjustable parameters, even if those parameters are just fitting the data noise, the calculated F-ratio can be compared to tabulated values to assess the significance of the improvement in misfit. Our first null hypothesis is that the measured velocities have the same variance about the North American plate as they do about a different plate (that is, they are not better described by an Euler pole different from North America). The calculated F-ratio far surpasses the minimum value at the 99% confidence level to reject this null hypothesis, so we conclude that the motion of the Bering plate relative to North America is significant at the 99% confidence level.

Next, we analyze each Aleutian region in the same manner and find that the Fox Islands region is eliminated from the Bering plate based on the F-test. We have no tectonic reason to believe that the Fox Islands do not lie on the Bering plate, but we think the arc velocity inversion there is poorly constrained and may be systematically biased because of the narrow trench normal range of measurements. We further investigate the arc velocities by calculating the Bering plate Euler pole with the omission of each region (Figure 3.11 and Table 3.2). We also test a two-plate model in which velocities from the

Aleutian arc are on a different plate than sites to the north, and an F-test reveals that there is not a significant improvement in the two-plate model.

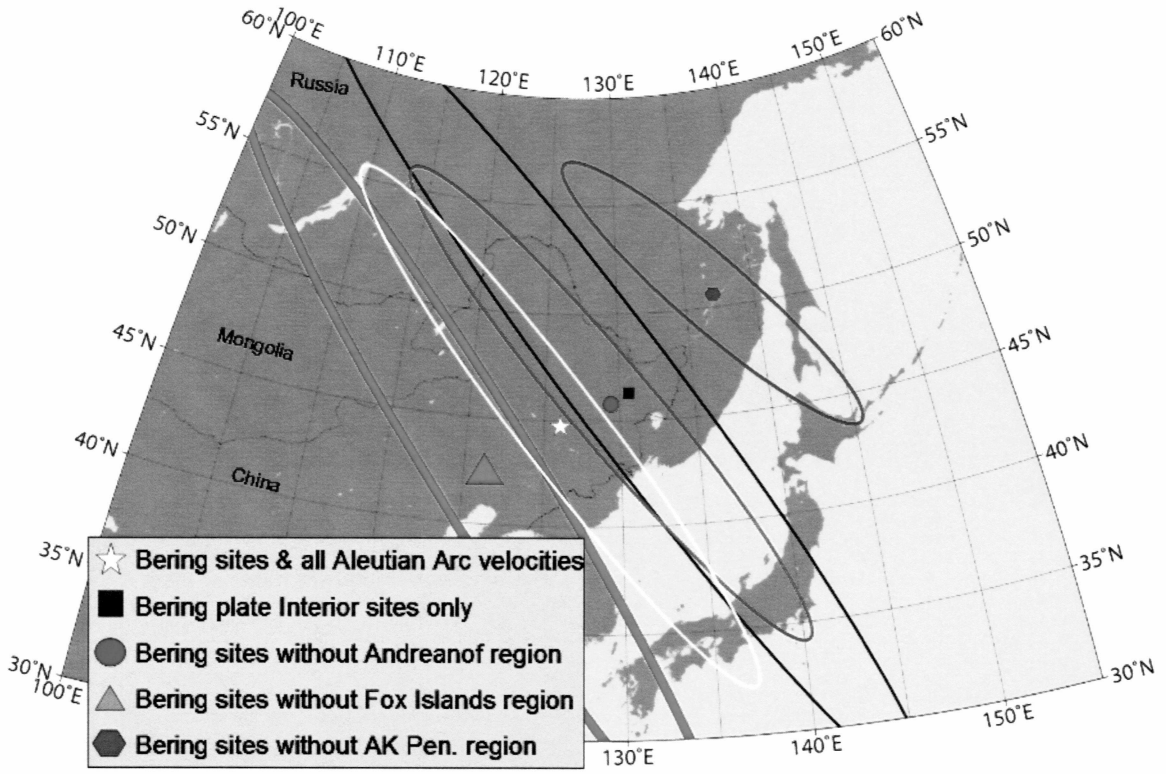

Figure 3.11 Map showing Bering plate Euler pole locations. Locations of possible Euler poles for the Bering plate relative to the North America plate. Ellipses represent 95% confidence regions for pole location. Euler pole location depends on which subset of GPS sites are included in the inversion. F-tests reveal that the Fox Islands region has a motion significantly different from the Bering plate. A quantitative comparison of Euler poles is giving in Table 3.2. The preferred model is shown by the large pink triangle.

Table 3.2 Bering plate Euler pole comparison table. The Euler pole vector is in an Earth centered Cartesian coordinate system in units of deg/my, such that the length of the vector is the angular velocity. Latitude and Longitude are in decimal degrees and ω is in degrees per million years. The best Euler pole is shown in bold.

							Pole vector		
Pole (data used)	**Symbol**	**Lat.**	**Long.**	**Ω(deg/my)**	**σω**	**red. χ^2**	**X**	**y**	**z**
Bering sites & all Aleutian Arc velocities	green star	44.74	126.05	6.8	2.5	3.12	2.8276	-3.8841	-4.7606
Bering plate Interior sites only	Black square	46.31	130.59	6.9	4.7	1.29	3.1153	-3.6361	-5.0119
Bering sites w/o Andreanof arc velocity	red circle	45.80	129.42	7.0	2.7	3.15	3.0752	-3.7417	-4.9809
Bering sites w/o Fox Islands arc velocity	**pink triangle**	**42.46**	**121.33**	**6.0**	**2.6**	**1.58**	**2.2978**	**-3.7744**	**-4.0434**
Bering sites w/o AP Pen. arc velocity	blue hexagon	50.60	137.60	8.8	3.1	3.25	4.0970	-3.8151	-6.8143

Based on the results of our F-test evaluations, we use the Euler pole based on sites in the plate's interior and the translation velocities from the Andreanof and Alaska Peninsula regions in further analysis of the Bering plate and its boundaries. This pole, which is located in Northeastern China, has an angular velocity of 6^{o}/my (Figure 3.11, Table 3.2). Using this Euler pole, we can compare the measured velocities and the arc translation velocities to the predicted velocities (Figure 3.12). Sites on the Bering Sea islands and Seward Peninsula are in very good agreement with the predicted velocities All predicted velocities fall within the 95% confidence region of the measured velocity being compared.

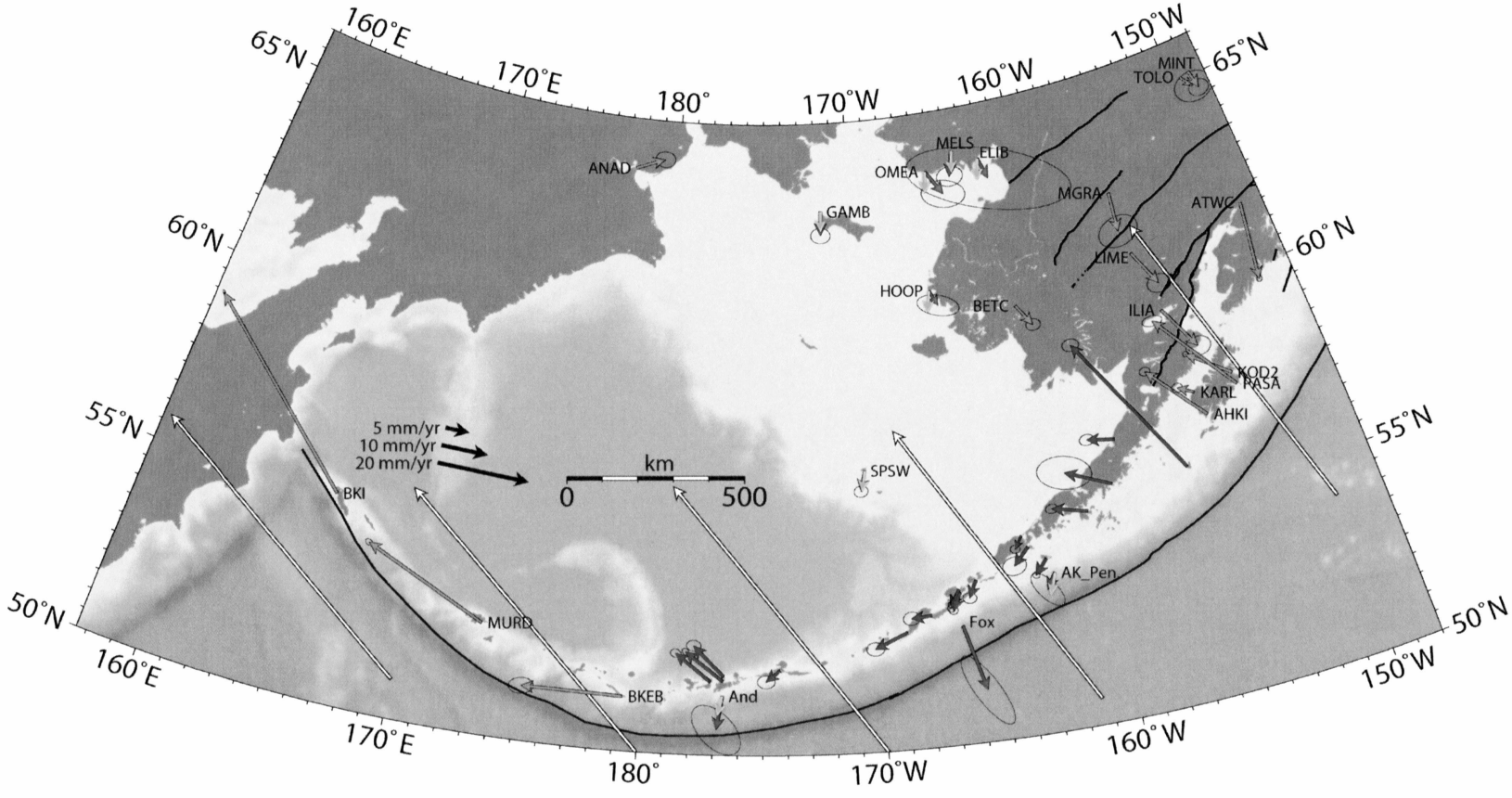
160°E
170°E
180°
170°W
160°W
150°W
65°N
60°N
55°N
50°N
ANAD
GAMB
MELS
ELIB
OMEA
MGRA
ATWC
MINT
TOLO
LIME
HOOP
BETC
ILIA
KODZ
PASA
KARL
AHKI
SPSW
AK_Pen
Fox
BKI
MURD
BKEB
And
5 mm/yr
10 mm/yr
20 mm/yr
km
0
500

Figure 3.12 Map of measured and modeled velocities for the Bering plate. Velocities for the Bering plate and surrounding areas are relative to North America. See Figure 3.1 for geographic names. Blue vectors are measured velocities on the Aleutian arc and the Alaska Peninsula. Pink vectors are velocities for sites located on the Bering plate interior that are used in the Euler pole inversion. Arc translation velocities calculated in Sections 3.4.2 to 3.4.4 are shown as red vectors. Yellow vectors are the velocities predicted for the Bering plate. Long white vectors represent Pacific plate velocities. All other measured sites are shown as grey vectors. Note that not all sites for the Aleutians and central Alaska are shown to avoid clutter. Sites west of the Andreanof Islands region show a clear acceleration of the arc, indicating that slip partitioning is an important mechanism contributing to the measured velocities of sites west of Amchitka Pass (180^{o} W).

3.6 Discussion

3.6.1 Fox Island Region Reassessment

The modeling results for the Fox Islands region were poorly determined because of a tradeoff between the arc translation velocity and coupling on the fault planes, and ultimately we chose not to use this region in our calculation of the Bering plate Euler pole. The Fox Islands region lies between the Andreanof and Alaska Peninsula regions which both behave as part of the Bering plate, thus we expect that the Fox Islands also lie on the Bering plate.

We predict the Bering plate velocity in the Fox Islands region using the other data and use this to reassess the coupling on the subduction interface. The predicted Bering plate velocity for the Fox Islands region is 1.4 mm/yr west and 4.7 mm/yr south. Using this arc translation velocity and the same fault geometry used in section 3.4.3 (Figure 3.8, Appendix 3.2), we obtain new coupling coefficients for the five fault planes (Table 3.3). The coupling coefficients are very different from the values predicted in Section 3.4.3, yet the reduced χ^2 value only increases from 4.16 to 6.04. The largest change is on plane 1, but this plane is the farthest from the data and is poorly constrained. When the arc velocity is constrained to the Bering plate predicted velocity, the estimated coupling coefficients become much smaller, however the uncertainties in the coupling remain large. This result seems much more realistic considering that, with the exception of ROWD and UNAL, the measured velocities are similar to the Bering plate motion. Data from new GPS sites spanning a larger trench-normal distance, or independent data from other sources would be required to improve the estimate of plate coupling in this region.

Table 3.3 Coupling coefficients and arc translation velocities for the Fox Island region. The new results use the predicted Bering plate velocity as the arc translation velocity.

	New	Previous
Plane 1	0%	100%
Plane 2	0%	90%
Plane 3	46%	100%
Plane 4	12%	10%
Plane 5	0%	0%
Arc velocity (E)	-1.4	3.6
Arc velocity (N)	-4.7	-14.3

3.6.2 Near Islands

The Near Islands is another region of the Aleutians with a sufficient number of GPS measurements to develop a fault model. There are six sites on Attu and one site on Shemya in the Near Islands (Figure 3.13, Appendix 3.1). These sites have been surveyed over as much as a ten-year timespan, but unfortunately a M_w 7.7 earthquake occurred 100 km southwest of Amchitka Island in November of 2003. This event caused large displacements on Amchitka and small displacements on Attu, so we have considered only pre-earthquake data in our analysis.

The convergence direction between the Pacific plate and the North American plate in the Near Islands region is very oblique; in fact, the convergence direction is only 10° away from being arc parallel (14 mm/yr trench normal convergence). Yet very large thrust events such as the 1965 (M_w 8.7) Rat Islands earthquake ruptured both the Rat Islands and Near Islands regions, an along strike distance of 600 km, indicating that subduction is active throughout this region. We construct a simple fault geometry with

one fault plane (Appendix 3.2). The top of the fault plane is located at the trench, the dip is set to 14° and the width is optimized at 120 km. Using the same grid-search inversion procedure as before, we solve for the coupling on the fault plane and a translation velocity of the Near Island region relative to North America using the seven sites from Attu and Shemya.

We find a coupling coefficient of 62% and an arc translation velocity of 14.4 mm/yr west and 2.3 mm/yr north (Figure 3.13). By subtracting the arc translation velocity from the Pacific-North America convergence velocity, we find the actual trench normal convergence rate is 19 mm/yr. This higher rate of trench normal convergence helps explain the existence of large thrust events in a region that appeared to have very oblique subduction. The coupling coefficient estimated for this region is 62±20%, signifying that a large portion of the interface is accumulating strain. *Beck and Christensen* [1991] used P waves to identify three regions of concentrated moment release for the 1965 Rat Island earthquake, and these regions were interpreted as asperities. One of these regions, 60 km wide, was located south of Agattu Island in the Near Islands region and corresponds to the region of our data (Figure 3.13).

We do not suppose that our estimated translation velocity for the Near Islands region is representative of Bering plate motion. Velocities measured on Amchitka and in the Near Islands have a significantly larger component of arc parallel motion than velocities recorded in the central Aleutians. It has been proposed, and our data support, that slip partitioning with right-lateral strike-slip faulting in the back-arc is a dominant factor in arc translation west of Amchitka Pass at 180°W [e.g. *Geist et al.,* 1988; *Ekstrom*

and Engdahl, 1989]. Thus, the translation velocity determined for the Near Islands represents both Bering plate motion and translation of the arc relative to the Bering plate. We subtract the predicted Bering plate velocity for the Near Islands, 0.1 mm/yr west 2.3 mm/yr south, from the translation velocity to obtain the velocity of the arc relative to the Bering plate. This velocity is 14.3 mm/yr west and 4.6 mm/yr north, and as we should expect, this velocity is close to arc parallel (14.7 mm/yr arc parallel, 3.2 mm/yr arc normal). This velocity represents the slip-partitioning rate on a strike-slip fault in the back arc. A fault in the back arc is most likely located at the bathymetric break or lineation only 20 km northeast of Shemya.

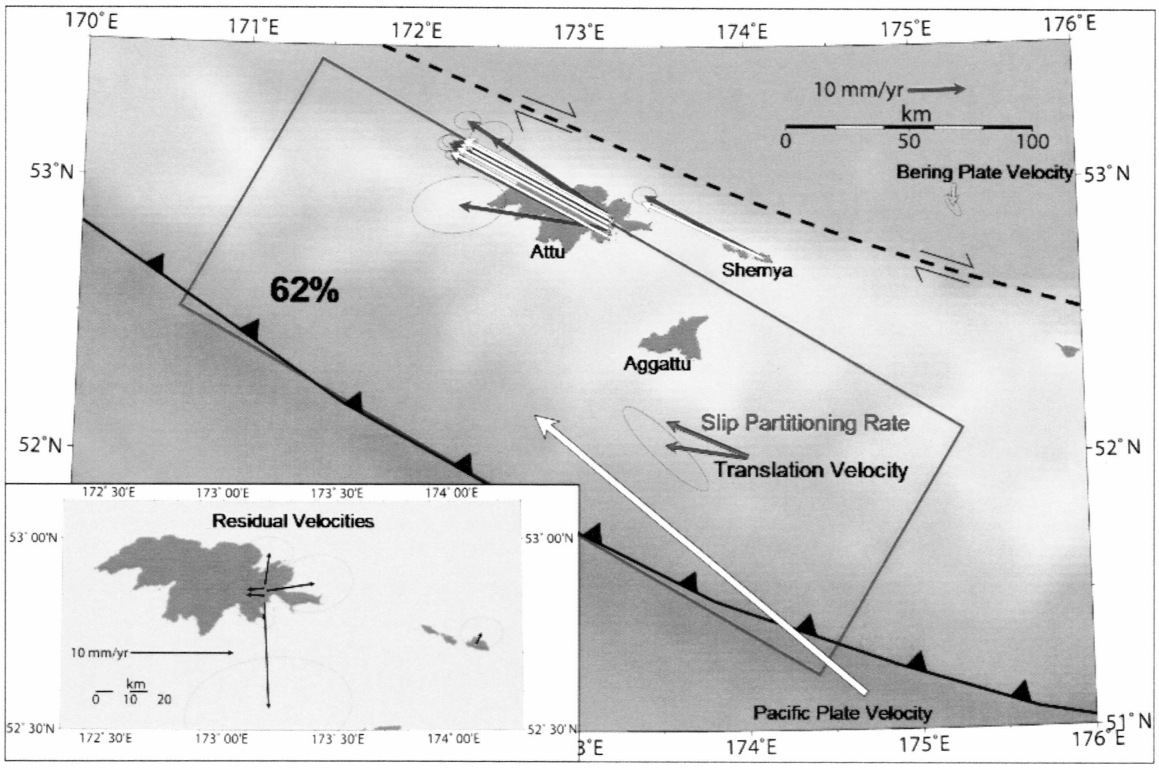

Figure 3.13 Fault plane geometry and geodetic modeling results for the Near Islands. Measured (blue) and modeled (white) velocities are relative to North America. The red vector is the translation velocity of the arc relative to North America calculated using the grid-search inversion procedure. The yellow vector is the Bering plate motion relative to North America. Pink vector is the arc translation velocity minus the Bering plate velocity and represents the motion of the arc relative to the Bering plate. This velocity represents the rate of arc parallel slip partitioning between the subduction zone and a strike-slip fault in the back-arc. The dashed line indicates the approximate location of a right-lateral strike-slip fault in the back-arc. Inset shows residual velocities for sites on Attu and Shemya; note the velocity scale is larger.

3.6.3 Rat Islands and Komandorsky Islands

In the Rat Islands, there is only one pre-2003 velocity (pre-earthquake). This site, BKEB, on Amchitka Island has a velocity of 19.8 mm/yr west and 0.6 mm/yr north (Figure 3.14). This velocity is nearly twice the velocity measured on Adak and Kanaga Islands 250 km to the east, indicating that slip partitioning has become an important mechanism here in the translation of the arc. We use the fault plane geometry for the Near Islands and adjust the strike for the Rat Islands region to solve for the arc translation velocity and the coupling on the fault plane. This inversion is not overdetermined as it was in previous calculations. Because it is equally determined we cannot give the uncertainty limits in our results. Nonetheless, we find an arc translation velocity that is 15.5 mm/yr west and 4.4 mm/yr south and the coupling coefficient for the single fault plane is 24%. In an effort to quantitatively analyze arc parallel extension using the GPS data, we test the assumption that the slip partitioning rate for the Near Islands can be applied to the Rat Islands region (i.e. there is no arc parallel extension between the two locations). Making this assumption, we can still fit the data on Amchitka within its 95% confidence limits, so we conclude that a model in which the Near Islands and the Rat Islands translate as a single block is permitted by our data. This result does not necessarily rule out arc parallel extension between the Rat Islands and the Near Islands, but only tells us that such extension in not required by the limited data we have.

On Bering Island in the Komandorsky Islands, the site BKI has been operating almost continuously since 1997. This well determined velocity is 49.5 mm/yr arc parallel, 18.6 mm/yr faster than the site MURD in the Near Islands (Figure 3.14). We

apply the same methodology used on the Rat Islands to the Komandorsky Islands, and find an arc translation velocity of 26 mm/yr west and 30 mm/yr north, with a coupling coefficient of 40%. This arc velocity is 80% of the observation at site BKI, leaving the other 20% to be due to interseismic strain. We again assume that the slip partitioning rate calculated for the Near Island region can be applied to the Komandorsky Islands to test arc parallel extension. We find that with this assumption we can no longer fit the data within its 95% confidence regions. This result indicates that there is significant arc parallel extension between the Near Islands and the Komandorsky Islands.

We use the arc parallel components of the arc translation velocities to calculate the strain rates between regions in the western Aleutians. Between the Komandorsky Islands and the Near Islands, the average arc-parallel strain rate is -4.8×10^{-8} yr^{-1} and between the Rat Islands and the Andreanof Islands the strain rate is -7×10^{-8} yr^{-1}. This strain must be accommodated either by normal faulting in the arc or by strike-slip faults that transition from the forearc to the back-arc, or by both mechanisms. An investigation of strike-slip earthquakes along the arc west of the Andreanof region, recorded in the Harvard CMT catalog, reveals the predominance of strike-slip events located in the back-arc (Figure 3.14). One cluster of strike-slip events located at 175° to 178° E shows an orientation rotated clockwise from the axis of the arc, which we believe may represent a fault or series of faults that cross from the forearc to the back-arc. The CMT catalog reveals no normal events at the appropriate depths and orientations to indicate extension in the arc by this mechanism.

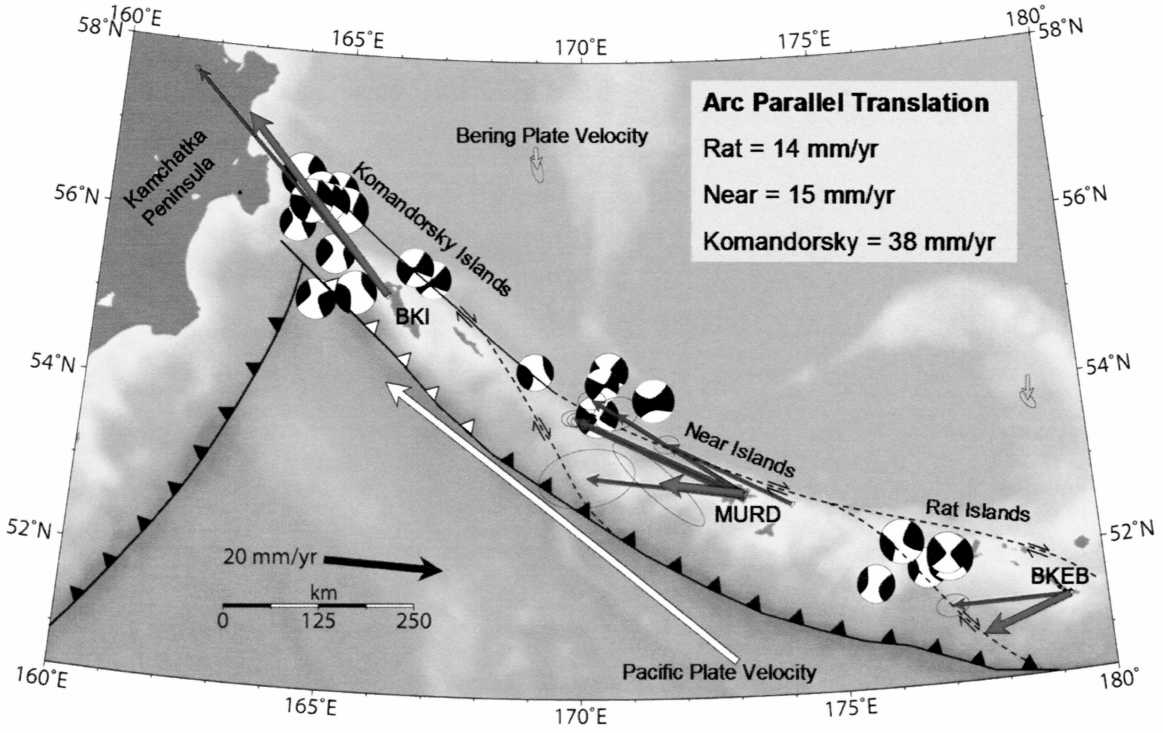

Figure 3.14 Measured GPS velocities in the western Aleutians. All velocities are relative to North America, including the velocity of the Pacific plate (white vector) and Bering plate (yellow vectors). Moment tensors of strike-slip events are from the Harvard CMT catalog. The cluster of events between the Rat Islands and the Near Islands may indicate a strike-slip fault that jumps from the forearc to the back-arc. The approximate locations of strike-slip faults are shown with a dashed line and arrows indicate the relative motion across the fault. Thrust faults are shown with teeth on the overriding plate, open teeth drawn for the far western Aleutians indicate a thrust fault where there is no trench normal convergence.

3.6.4 Earthquake Slip Azimuths

An independent method for examining slip partitioning is to use slip azimuths from thrust earthquakes along the Aleutian arc. We use the Harvard CMT catalog to find all Aleutian thrust events from 1976 to 2007. We use the following parameters to constrain the events: depth < 50 km, dip < 30°, strike 200° to 300°, rake 30° to 150°, and all events must fall along the arc. These thrust azimuths are then compared to the Pacific-North America convergence direction based on the REVEL plate motion model [*Sella et al.*, 2002] and the Pacific-Bering convergence direction (Figure 3.15).

Following *Ekstrom and Engdahl* [1989], we consider a simple model of slip partitioning in which the relative plate motion is accommodated by slip on the main thrust zone and strike-slip motions on a vertical fault plane coincident with the arc. We assume that the strike-slip motions occurring on a vertical plane are proportional to the local projection of the Pacific relative to Bering plate motion vector onto a line following the strike of the arc. We can then define

$$V_{ARC-BR} = k \cdot \cos(\phi - \theta) \cdot V_{PC-BR} \qquad (3.6.1)$$

where V_{ARC-BR} is the velocity of the arc relative to the Bering plate, V_{PC-BR} is the Pacific-Bering plate convergence velocity with azimuth ϕ, θ is strike of the arc, and k is a proportionality constant that specifies what fraction of the arc-parallel relative plate motion is partitioned on to the strike-slip faults. For no partitioning, k=0, and for full partitioning, k=1. The azimuth of convergence across the main thrust zone becomes

$$\psi = \frac{\pi}{2} + \theta - \tan^{-1}\left(\frac{(1-k)\cos(\phi-\theta)}{\sin(\phi-\theta)}\right) . \qquad (3.6.2)$$

This should be the same as the slip azimuths for thrust events. A value of $k = 0.55 \pm .03$ provides the best fit to the earthquake slip azimuths. This is slightly lower than the value of 0.6 obtained by *Ekstrom and Engdahl* [1989], but they did not consider the motion of the Bering plate relative to North America, as it had not yet been recognized quantitatively, and their data set was considerably smaller.

Using this value of k we calculate the velocity of the arc relative to the Bering plate based on equation 3.6.1 (Figure 3.15). This calculation shows that the velocity of the arc relative to the Bering plate should be zero at 158° W, where Pacific-Bering plate convergence is normal to the trench. At 170° W, slip azimuths indicate that slip partitioning should be approximately 20 mm/yr, yet our geodetic modeling of the Andreanof region data revealed trench parallel arc velocity of only 0.8 mm/yr relative to the Bering plate.

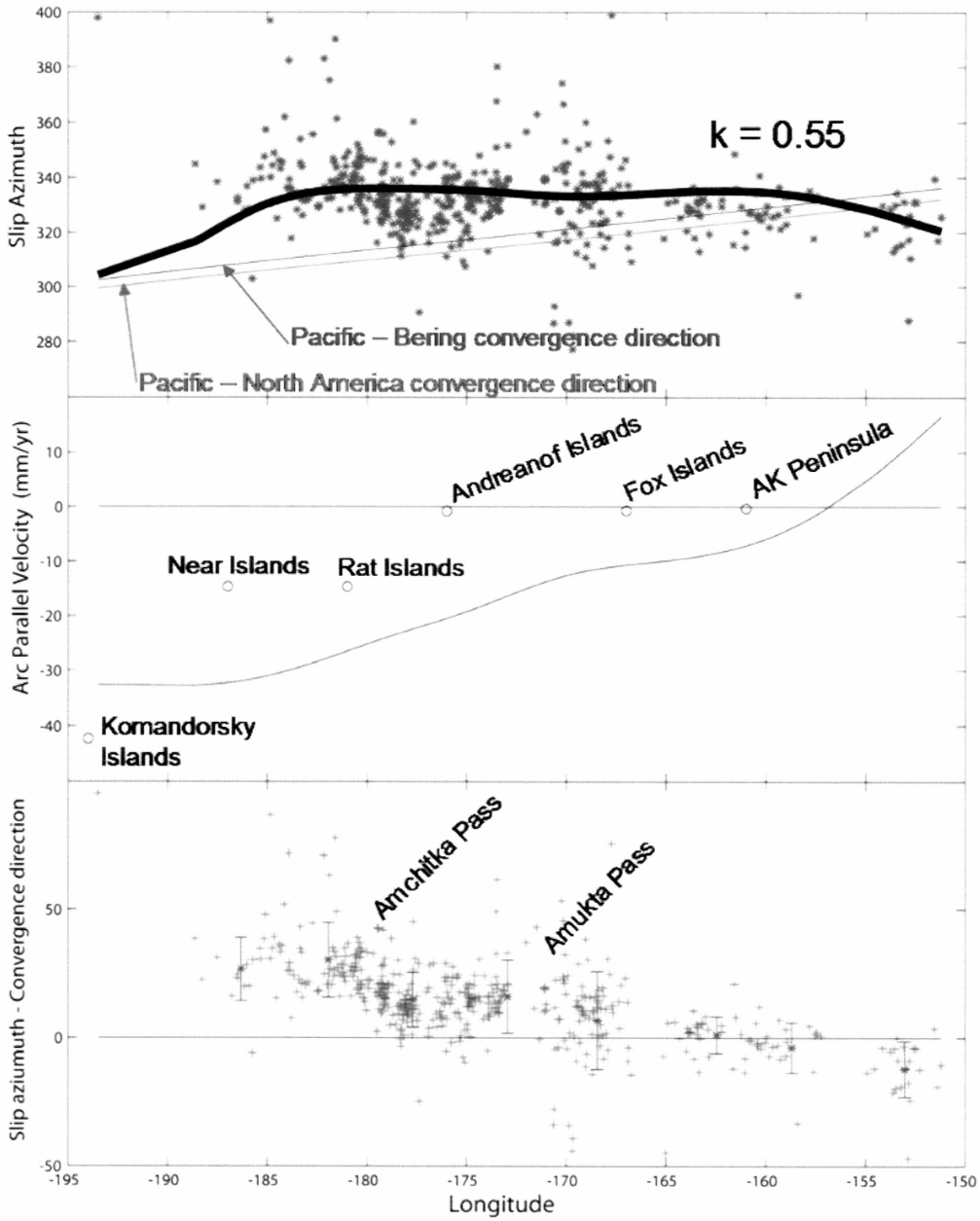

Figure 3.15 Plots examining Aleutian arc parallel translation. (Top) Thrust earthquake slip azimuths and plate convergence directions vs. longitude for thrust events, green line is the Pacific-North America convergence direction and red is the Pacific-Bering plate convergence direction. Thick black line is the convergence direction based on the model described above with k = 0.55. (Middle) Arc parallel translation of the arc relative to

Bering plate based on slip azimuth, convergence direction and arc orientation. Circles are the arc parallel translation velocities based on GPS measurements (relative to the Bering plate). (Bottom) Slip azimuth minus Pacific-Bering plate convergence direction vs. longitude. Average is shown for 5° bins of longitude with one standard deviation error bars. Note the 15.4° jump at Amchitka Pass and 9.1° jump at Amukta Pass.

The large discrepancy between the geodetic observations and the slip vector azimuths can be explained if slip partitioning in the eastern Aleutians involves faults entirely in the forearc. *Ryan and Scholl* [1989] used seismic reflection data to identify major arc parallel shear zones in the forearc, such as the Hawley ridge shear zone south of the Andreanof Islands. These shear zones may partition slip from the subduction interface such that the slip vector on the trench side of these faults is more normal to the trench than the convergence direction on the arc side of the faults farther down the interface. For simplicity, we can think of these shear zones as a single arc parallel strike-slip fault. If the faults in the forearc are arc slipping freely, we would expect to record a step in the trench parallel strain across these faults. Unfortunately, GPS measurements cannot record the rapid arc parallel motions in the forearc because these faults are inaccessible beneath the ocean.

The other possibility is that the strike-slip faults in the forearc are locked interseismically. *Darby and Beavan* [2001] used a dense network of GPS measurements on the southern tip of North Island, New Zealand, to show that strain in the upper crust resulting from oblique subduction is completely explained by an elastic deformation model with oblique slip on the plate interface even when there is geologic evidence for

major slip partitioning on strike-slip faults. In other words, the instantaneous interseismic GPS measurements record the same deformation in the case of no slip partitioning with case of locked strike-slip faults in the forearc. We have constructed a simple dislocation model to investigate how this is possible. The assumptions of the Savage model are that the interseismic deformation can be represented by the superposition of steady state subduction along the entire plate interface (forward slip), and steady normal slip (back slip) in the main thrust zone at the plate convergence rate. This results in a plate interface that has a locked main thrust zone and is slipping freely above and below this zone [*Savage,* 1983] (Figure 3.2). In reality, we normally assume that the forward slip produces no deformation in the locked zone and thus it is not necessary to construct this part of the model. In the case of slip partitioning of the forearc, we can no longer make this assumption as the forward slip does produce deformation, and we have included forward-slip in the model using the elastic subducting plate model proposed by *Kanda and Simons* [2006] (Figure 3.16).

We attempt to make the model reasonably realistic while retaining simplicity and use parameters that are representative of the Aleutian subduction zone. The simple model consists of a dipping slab with an effective elastic thickness of 22 km, based on the effective thickness of 60 Ma oceanic crust [*Watts et al.,* 1980]. The convergence is set at 50 mm/yr in both the trench normal and trench parallel directions. A vertical trench-parallel strike-slip fault is located 50 km from the trench with a locking depth of 5 to 23 km (Figure 3.16). The slip rate on this fault is half of the trench parallel convergence (25 mm/yr) (i.e., 50% partitioning in the forearc). We divide the thrust interface into two

parts, the upper section where there is only half the trench parallel slip rate and a lower section where there is full plate convergence velocity. Furthermore, in the forward slip part of the model we include slip at the convergence velocity at the bottom of the elastic lithosphere. This lower dislocation approximates the motion of the downgoing plate in a frame in which the overriding plate is fixed. We compare this model to the simple back slip model with no strike-slip faults. We observe that within the region of potential observations (~130 km or more from the trench) there is no more than a 1.9 mm/yr difference between the two models (Figure 3.17). A 2 mm/yr difference in GPS measurement is likely to be undetected or attributed to some other parameter such as dip angle, coupling on the main thrust or the arc velocity.

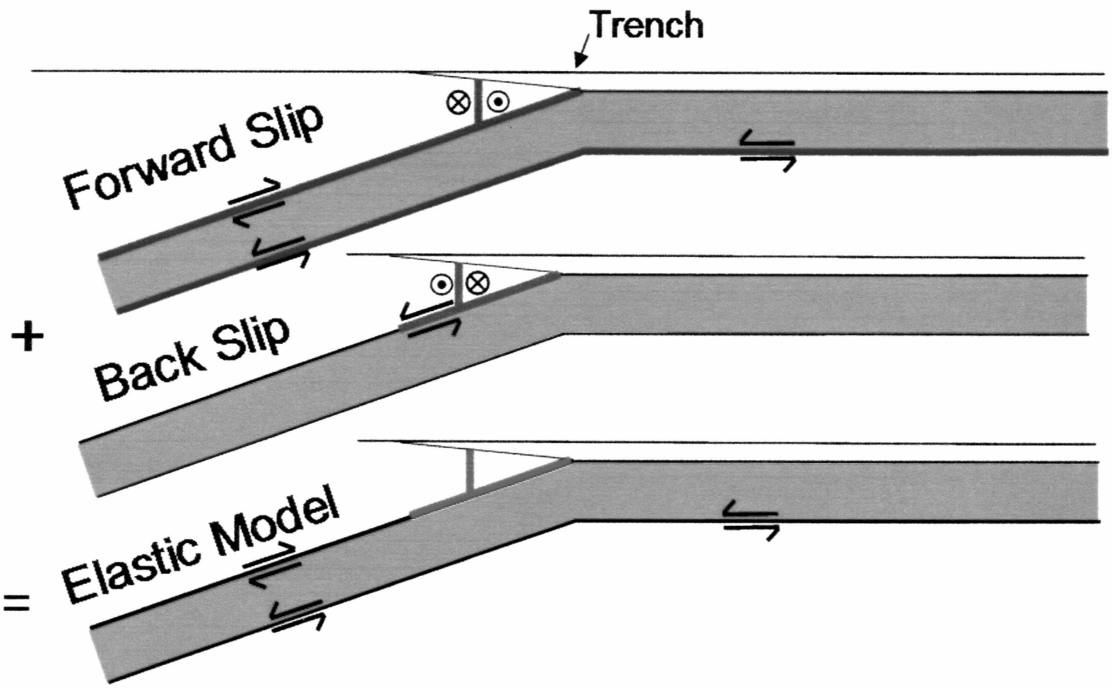

Figure 3.16 Schematic cross-section of the elastic slip partitioning model. This model is used to examine a locked strike-slip fault in the forearc. The model is slightly different from previous models in that we calculate the effects of forward slip of the subducting slab relative to the overriding plate. The model is compared to the standard back slip model, a model that is identical to the back slip component of this model but without the strike-slip fault. Red region in the elastic model represents the locked zone where no slip occurs in the interseismic periods.

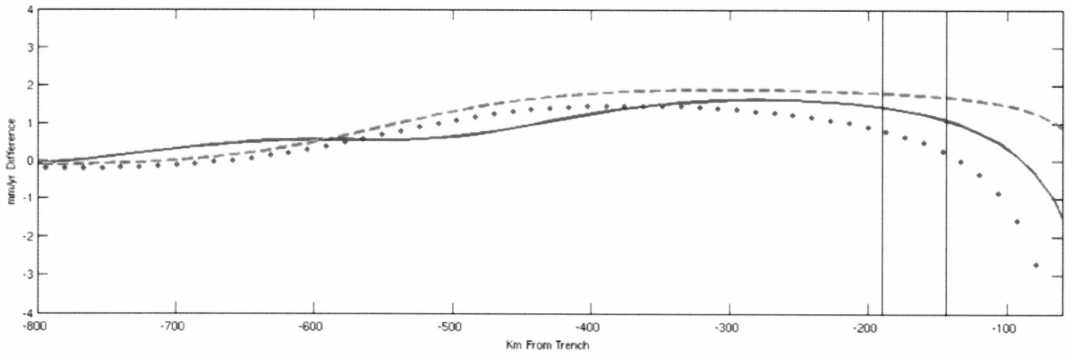

Figure 3.17 Plot of difference between back slip and partitioned slip models. Solid red line is the trench normal difference, which is not affected by whether the strike slip fault is locked, or not. The green dashed line is the trench parallel difference between a partitioned model with a locked strike-slip fault and a normal model with oblique back slip. The dotted blue line is the trench parallel difference between a partitioned model with a freely slipping strike-slip fault and the normal model with oblique back slip. The two vertical lines represent the trench normal range of distances of measurements made in the Aleutians.

In the case of the Aleutians, we have evidence from thrust-earthquake slip azimuths that there is slip partitioning in the forearc, but our data cannot resolve whether these faults are locked or creeping. We can say with certainty that east of Amchitka Pass, slip partitioning is not active in the back-arc (Figure 3.18). This is different from previous studies such as *Ekstrom and Engdahl* [1989] that suggested slip partitioning in the back arc was a major tectonic component of the central and eastern Aleutians. It is not possible to resolve the discrepancy between thrust azimuths and GPS measurements with a model in with slip partitioning is constrained to the back-arc.

We have calculated an arc parallel translation rate of the forearc based on slip vector azimuths, and an arc parallel translation of the main arc based on GPS

measurements (Figure 3.15 middle). The difference between these velocities is the slip rate on strike-slip faults in the forearc. We can calculate approximate recurrence intervals by assuming that these faults are locked and rupture periodically in large earthquakes that produce 2-5 meters of displacement (M_w 7-7.5). In the central Aleutians, the slip rate is approximately 20 mm/yr, giving a recurrence interval of 100 to 250 years, and in the eastern Aleutians, the slip rate is 10 mm/yr, giving a recurrence interval of 200 to 500 years. We have at most been recording earthquakes in the Aleutians for 50 years, so it is possible that we have simply not yet recorded one of these large strike-slip events in the forearc.

We subtract the slip azimuths from the Pacific-Bering convergence direction and group events into bins of 5° longitude and calculate the mean difference and standard deviation (Figure 3.15 bottom). This calculation reveals a jump in slip azimuth of 15.4° at approximately 180° W, corresponding to Amchitka Pass and Sunday Basin, where we believe slip partitioning becomes active in the back-arc as well as the forearc based on GPS measurements. The next largest change in slip azimuth is 9.1° and occurs at approximately 170°W (Amukta Pass). This region corresponds to the Amlia and Amukta basins, which like the Sunday basin are interpreted to have evolved from the westward dismemberment of the arc via block translation and rotation [*Geist et al.,* 1988].

A model that may explain our observations would be one in which slip partitioning in the forearc increases with the steady increase of obliquity of subduction, but slip partitioning also involving the back-arc begins at discrete locations and thus

results in step like changes in thrust-earthquake slip azimuth when plotted against their along strike location (Figure 3.18).

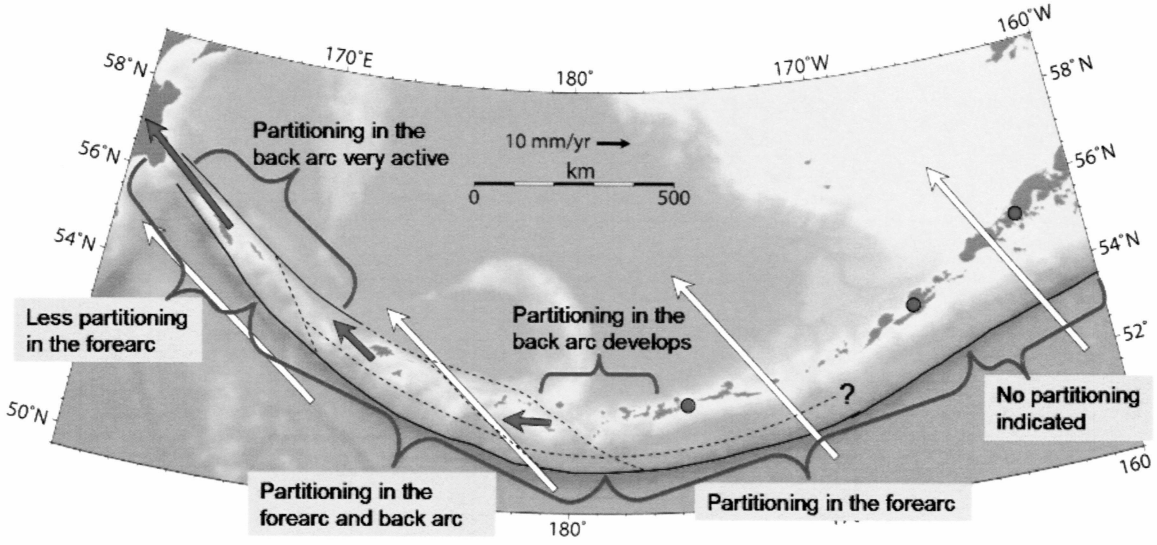

Figure 3.18 Map of slip partitioning regions of the Aleutian arc. The red vectors are the arc parallel components of the arc translation velocities relative to the Bering plate. Red dots indicate regions in which there is no motion relative to the Bering plate. Pacific plate velocities are shown as the white vectors. The trench of the Aleutian subduction zone is shown as a thick black line. Strike slip faults are indicated by thinner black lines and are dashed where they are approximately located.

3.7 Boundaries of the Bering Plate

With the recognition of a new plate comes that realization that some regions previously considered to be part of a plate's stable interior are in fact active plate boundaries. The previous sections were devoted to discussing the tectonics of the Aleutians, the southern boundary of the Bering plate. In the following sections, we focus on the remaining boundary zones in western Alaska and eastern Russia.

3.7.1 Eastern Bering Plate Boundaries

Measurements from western Alaska show a southwestward velocity that is clearly distinct from the North American plate and represents coherent Bering plate motion. Sites in the interior of Alaska, 500 km east of the Seward Peninsula, do not agree with the Bering plate motion (Figure 3.19). In November of 2002, the Denali fault earthquake (M_w 7.9) ruptured 327 km of the Denali fault system including parts of the Totschunda and Susitna Glacier thrust fault. This caused significant coseismic and postseismic deformation throughout much of the state, so we only consider pre-earthquake velocities for comparison with the Bering plate's predicted motion. The site CLGO in Fairbanks, Alaska has a well determined pre-earthquake velocity of 3.0 mm/yr directed southeast, which is different from the predicted Bering plate velocity of 5 mm/yr directed to the south-southwest. The sites BRWN and NENA have southward velocities that are not very different from the predicted velocities, but unfortunately these sites are not well constrained and we cannot put much confidence in interpreting them. The CGPS site GRNR, located 40 km south of BRWN, has a well-determined velocity and is similar to CLGO (Figure 3.19, Appendix 3.1). Farther to the east of Fairbanks, velocities are closer to the North American plate motion and we conclude that the eastern boundary of the Bering plate must lie somewhere between well-constrained sites on the west coast of Alaska and in the interior of the state.

Seismicity patterns may help us distinguish this boundary. One location with abundant seismicity is in the interior of Alaska north of the Denali Fault where multiple NNE trending seismic zones have been identified and where there have been at least six

M_w 6 and larger events in the last 100 years. These zones of shallow seismicity have previously been interpreted as bookshelf faulting (i.e. left lateral faults between clock-wise rotating blocks that develop between the larger east west striking right-lateral strike-slip Denali and Tintina faults) [*Page et al.,* 1995]. The most prominent of these seismic lineations in the westernmost, known as the Minto Flats seismic zone (MFSZ).

The MFSZ consistently produces earthquakes less than 30 km deep with near vertical and NNE striking fault planes. In 1995, the north segment of the MFSZ ruptured in a M_w 6.0 earthquake, and the best moment tensor for this event shows a strike of 208° and a dip of 74°E (Figure 3.19). *Ratchkovski and Hansen* [2002] used a catalog of 196 fault-plane solutions to calculate the principal stress directions in the crust in interior Alaska. They subdivided the study area into separate regions and found minimum and maximum horizontal stress directions (SH_{min} and SH_{max}). West of the MFSZ, *Ratchkovski and Hansen* [2002] found the SH_{min} is oriented 41°, whereas in the MFSZ it is oriented at 83°, and east of the MFSZ SH_{min} is 105°. Velocities predicted for the Bering plate relative to North America in interior Alaska are parallel to these seismic zones and to the SH_{min} west of the MFSZ, and Bering-North America relative motion would produce left-lateral faulting here.

We conclude based on the data available that the Bering plate is moving to the south-southwest relative to the North American plate causing the stress orientations calculated by *Ratchkovski and Hansen* [2002]. The seismic zones in the Interior probably represent the eastern limit of a diffuse North America-Bering plate boundary zone. The stresses may also be due in part to the subduction of the Pacific plate underneath the

North American plate, and this could be driving the westward extrusion of the Bering plate via block rotation and north-south crustal shortening in interior Alaska.

There are no reliable GPS measurements between the interior and the west coast of Alaska, thus we cannot say with certainty the location or size of the plate boundary between these two locations. With the data available, it appears that the eastern boundary of the Bering plate is a diffuse zone involving strike-slip faults, small block rotation, and extension but the lack of seismicity west of 152° W and south of the Kaltag fault indicates that the majority of the strain may lie closer to Alaska's interior.

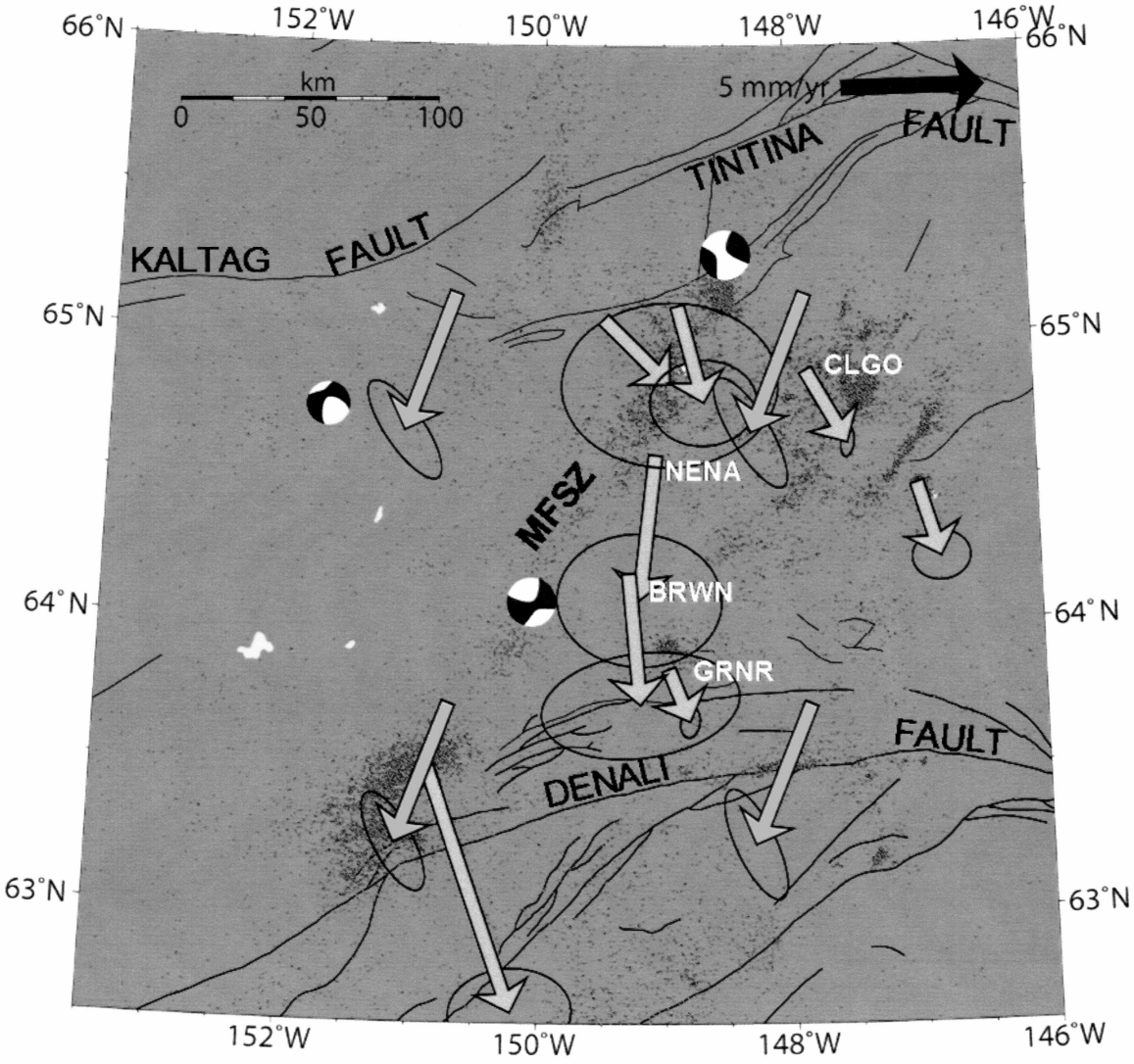

Figure 3.19 Map of Pre-Denali earthquake seismicity and GPS velocities. Earthquakes (grey dots) show three clear NNE lineations that are almost parallel to the velocities of the Bering plate relative to North America shown as yellow vectors. Thin black lines indicate mapped fault traces. Pre-Denali earthquake measured velocities are shown by the grey vectors.

The Denali fault is a major tectonic boundary that isolates the counter-clockwise block rotation of southcentral Alaska from the rest of the state. Pre-Denali earthquake GPS measurements from south of the Denali fault can be fit by an Euler pole located at 59.63°N, 147.38°W with an angular velocity of 0.77°/my ([*Fletcher*, 2002], Figure 3.20). The Denali fault continues west of the 2002 rupture area for over 400 km (as the Farewell fault), but the Holocene slip rate of the Denali fault is thought to decrease west of 150°W, and there have been no major earthquakes recorded along this western section [*Doser*, 2004]. One possible explanation for this behavior is the similarity of the velocities predicted for the Bering plate and the southcentral block in this region (Figure 3.20). If the Denali fault separates the Bering plate on the north from the southcentral Alaska block on the south, the rate of strike-slip motion would be very slow. In fact, on the Denali Fault at 155°W and 62°N the difference between the Bering plate prediction and southcentral Alaska prediction is 1.8 mm/yr and is parallel to the Denali fault with a right-lateral sense of motion. East of this point, there is a component of compression across the Denali fault, and east of 152°W there is a well-developed foreland fold and thrust belt north of the Alaska Range and Denali fault, which may accommodate this fault normal convergence (Figure 3.20).

A reasonable analogy is interlocking gears, where two gears of different sizes rotate about different axes at different angular velocities but their interaction causes no strain because they are moving at the same rate along their mutual boundary. This type of tectonic interaction exists in other locations, for example, the Sierra Nevada block with

the Oregon coast block [*Wells et al.*, 1998; *Williams et al.*, 2006], and the South China block with North China block [*Heki et al.*, 1999].

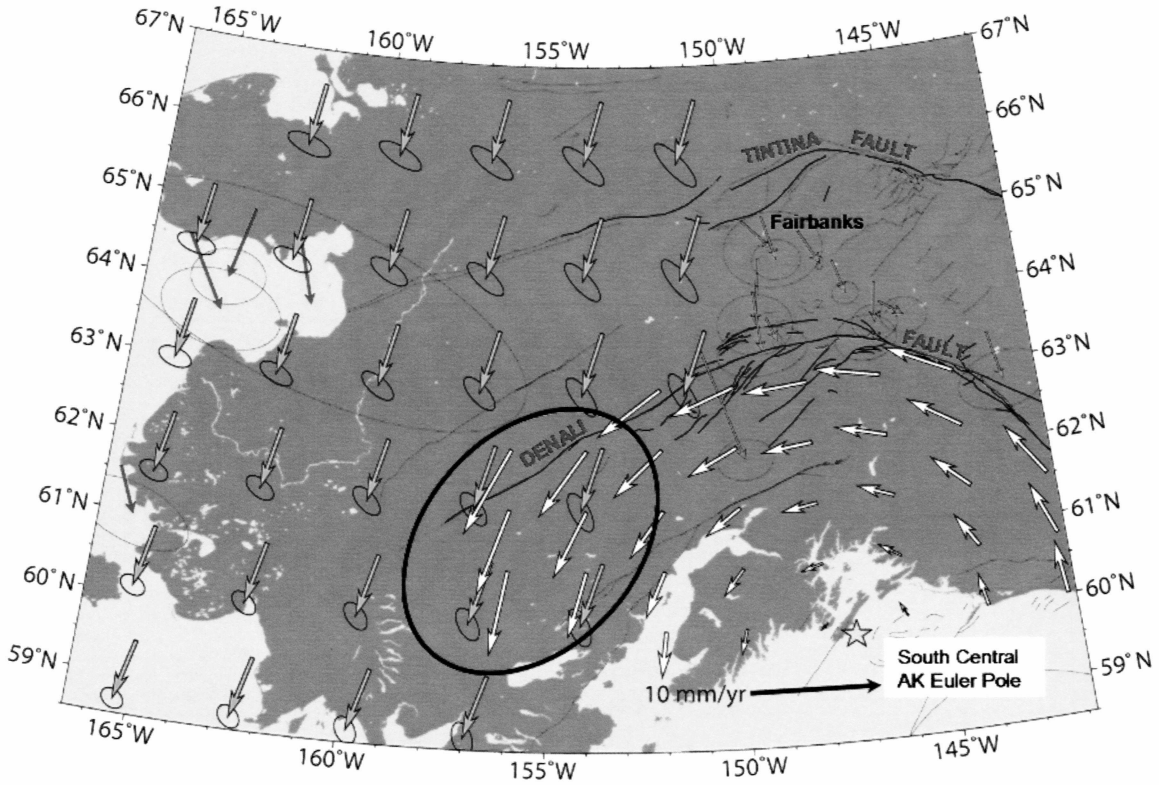

Figure 3.20 Plate velocity comparison map for interior Alaska. Yellow vectors represent the predicted velocity of the Bering Plate, and white vectors represent the southcentral Alaska block. Blue vectors are measured velocities of sites on the Bering plate and gray vectors are pre-Denali earthquake velocities of interior AK. Velocity of the Bering plate and the southcentral block are similar in the region of the ellipse near the western segment of the Denali fault. Measured velocities for southcentral Alaska are not shown due to complications involving interseismic strain and postseismic deformation from the 1964 Great Alaska Earthquake [*Zweck and Freymueller*, 2002].

3.7.2 Western Bering Plate Boundary

The western boundary of the Bering plate is assumed to be located in the Koryak Highlands, Russia, based on mapped faults and large earthquakes [*Mackey et al.*, 1997, *Fujita et al.*, 2002]. Using the Harvard CMT catalog, we have compared earthquake mechanisms to the few available GPS measurements from eastern Russia (Figure 3.21). Sites BILI and KMS show an east-southeast motion relative to North America, but the predicted motion of the Bering plate is south-southwest, thus we expect both contraction and northeast-southwest right-lateral shearing across this region. A cluster of primarily thrust events is located near the top of the Kamchatka Peninsula in the southern Koryak highlands. The GPS site TIL has a velocity of 7.7 mm/yr in a direction very similar to that predicted for the Bering plate. It is possible that the sites KMS and TIL are located on opposite sides of the plate boundary. Site ANAD has a northeast velocity of 6.6 mm/yr. This motion relative to the Bering plate should produce right-lateral faulting. In 1986, a M_w 5.3 event was recorded in the Gulf of Anadyr at approximately 170° E, 62° N. This event has a right-lateral fault plane solution with a strike of 245° and a near vertical dip (Figure 3.21). However, the site ANAD has only been surveyed twice with a one-year time span between occupations and thus its velocity may not be reliable yet, and may change with more occupations.

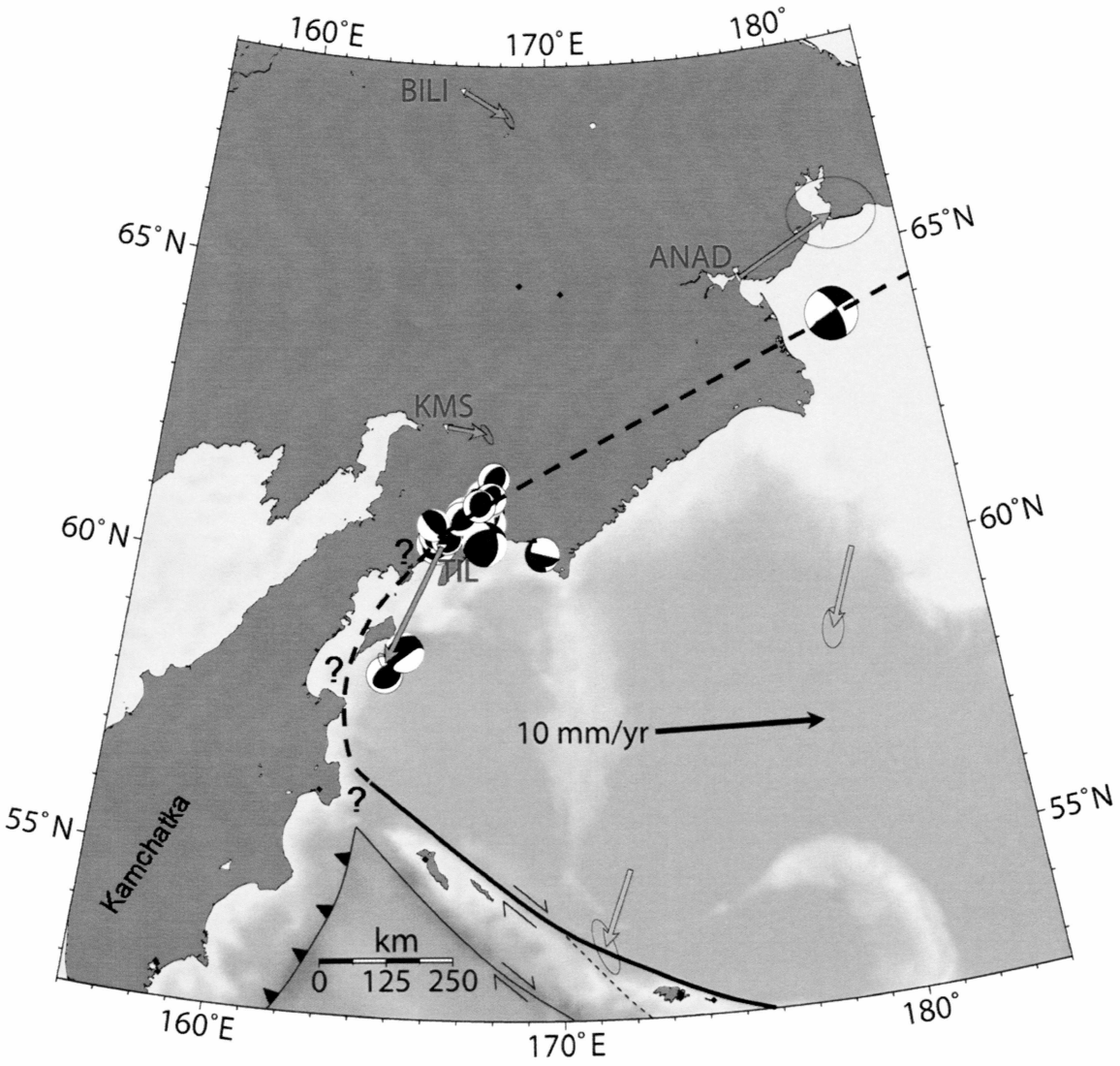

Figure 3.21 Map of GPS measurements and seismicity in eastern Russia. Thrust events are clustered in the Koryak highlands possibly the result of convergence between the Bering plate and eastern Russia. A M_w 5.5 earthquake is located at 178.7°W, 63.9°N and shows the appropriate right-lateral mechanisms for the relative motion between Bering plate (yellow) and site ANAD. Approximate boundaries of the Bering plate are shown as thick black line, regions of uncertainty are dashed and question marks indicate where the boundary location is unknown.

3.7.3 Northern Bering Plate Boundary

Based on seismicity, the northern boundary of the Bering plate is an extensional setting trending east-west through the Seward Peninsula. The boundary extends to the west and southwest through eastern Russia where it transitions into right-lateral strike-slip faulting before reaching the Koryak Highlands, which are dominated by thrust events [*Mackey et al.*, 1997; *Fujita et al.*, 2002]. The Seward Peninsula has well documented extension, including normal faults with Holocene offsets, geothermal activity, and young basalt flow deposits. To the east of the Seward Peninsula, there is less certainty in the Bering plate's boundary. We speculate that the plate boundary involves the Kaltag fault, as it is the most obvious feature that connects the Seward Peninsula to seismicity in Interior Alaska. The Kaltag fault has had at least two M_w 5 earthquakes in the last 30 years; both of these events were right-lateral with a minor component of extension.

There are no GPS measurements in the vicinity of the Kaltag fault and all measurements on the Seward Peninsula are south of the proposed boundary. The nearest reliable measurement to the north is site SG27 in Barrow over 800 km away. SG27 has a well-determined velocity of 1.3 mm/yr east and 2.8 mm/yr south (Figure 3.22). Although this site still has a significant southward velocity relative to North America, it is only half of the predicted Bering plate motion or the velocity of site MELS on the southern Seward Peninsula. As with the eastern boundary, the northern boundary may be a diffuse zone of deformation with localized regions of more intense deformation such as the Seward Peninsula. An increased network of geodetic measurements by the Plate Boundary

Observatory (National Science Foundation, Earth Scope initiative) will better constrain the plate's boundaries in the next few years.

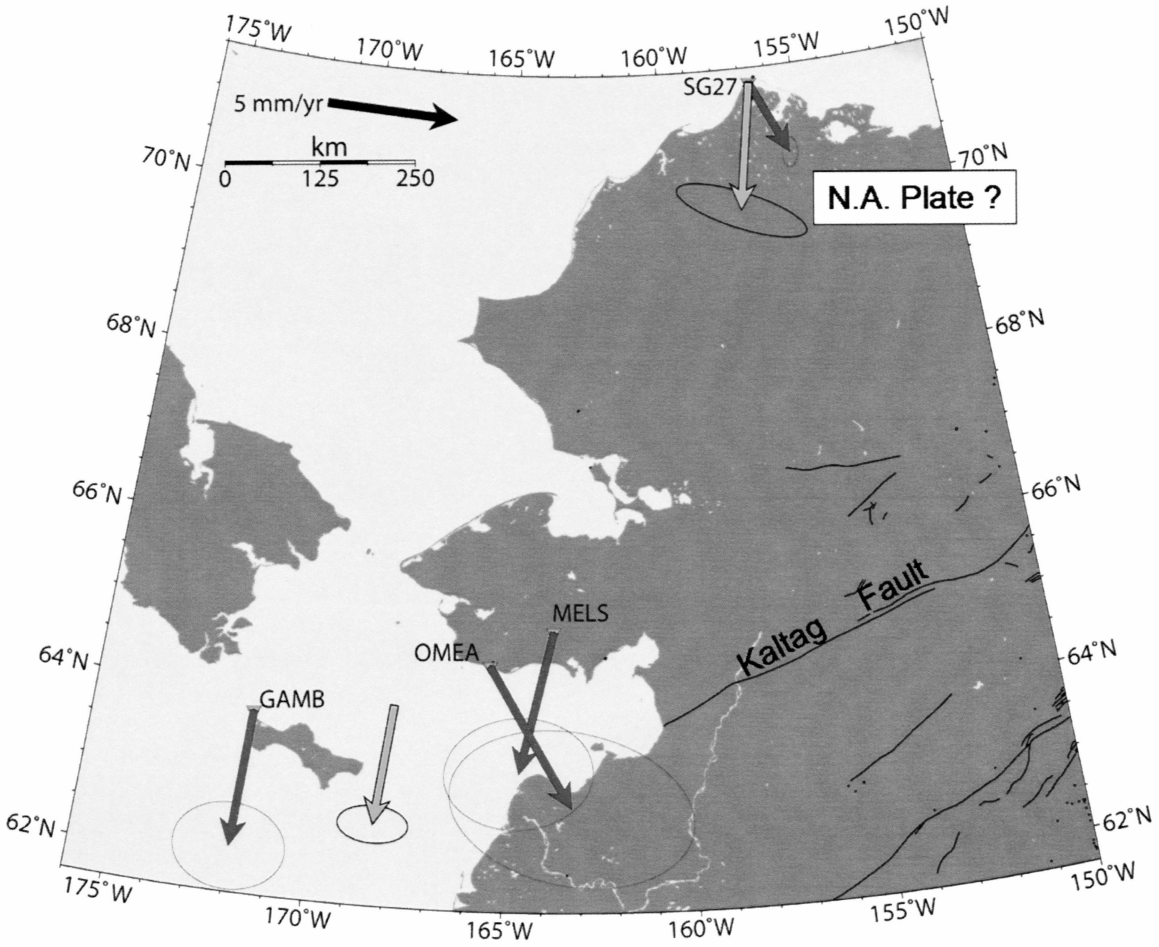

Figure 3.22 GPS velocity map of the northern boundary of the Bering plate. Measured velocities are shown in blue, predicted Bering plate velocities are shown in yellow. The velocity of sites SG27 in Barrow is significantly different from the Bering plate, but also very different from stable North America.

3.8 Summary

Using geodetic measurements from the Aleutians, western Alaska, and the Bering Sea islands, we have quantified the motion of the Bering plate. We find that the Bering-North America Euler pole is located at 42.5° N, 121.3° E with an angular velocity of 6.0°/my. GPS measurements along the Aleutian arc record an arc parallel acceleration west of Amchitka Pass indicating slip partitioning has developed in the back-arc. Elastic dislocation modeling reveals that, east of Amchitka, the arc moves uniformly as part of the Bering plate. Discrepancies between thrust earthquake slip azimuths and plate convergence directions are explained by strike-slip faults in the forearc.

The eastern boundary of the Bering plate lies between the west coast of Alaska and interior Alaska, with the most likely location being in interior Alaska based on seismicity patterns and focal mechanisms. Southwest motion of the Bering plate relative to North America may be responsible for the left lateral faulting in the Minto Flats Seismic Zone that connects the Denali fault to the south with the Tintina fault to the north, as part of a diffuse Bering-North America plate boundary zone.

Interaction between a clockwise rotating Bering plate and a counter-clockwise rotating southcentral Alaska block may be responsible for the reduced slip rate and lack of seismic activity on the western Denali fault, and for the development of a prominent foreland fold and thrust belt in the central Alaska Range.

We believe the western boundary of the Bering plate lies in eastern Russia and involves thrusting in the Koryak highland and strike-slip faulting farther to the northeast

that connects with the extension on the Seward Peninsula. GPS measurements from eastern Russia are sparse but support this hypothesis.

3.9 References

Beck, S. L., D. H. Christensen (1991), Rupture process of the February 4, 1965, Rat Islands earthquake, J. Geophys. Res., 96(B2), 2205-2221, 10.1029/90JB02092.

Boyd, T. M. and J. L. Nabelek (1988), Rupture process of the Andreanof Islands earthquake of May 7, 1986, *Bull. Seis. Soc. Amer.*, *78*(5), 1653-1673.

Cooper, A. K., M. S. Marlow, D. W. Scholl, and A. J. Stevenson (1992), Evidence for Cenozoic crustal extension in the Bering Sea region, *Tectonics*, 11(4), 719-731.

Cross, R. S., and J. T. Freymueller (2007), Plate coupling variation and block translation in the Andreanof segment of the Aleutian Arc determined by subduction zone modeling using GPS data, *Geophys. Res. Lett.*, In press.

Darby, D., and J. Beavan (2001), Evidence from GPS measurements for contemporary interpolate coupling on the southern Hikurangi subduction thrust and for partitioning of strain in the upper plate, *J. Geophys. Res.*, 106(12), 30881-30891.

Doser, D. I. (2004), Seismicity of the Denali-Totschunda fault zone in central Alaska (1912-1988) and its relation to the 2002 Denali Fault earthquake sequence, *Bull. Seis. Soc. Am.*, 94(6B), S132-S144.

Dumitru, T. A., E. L. Miller, P. B. O'Sullivan, J. M. Amato, K. A. Hannula, A. T. Calvert, and P. B. Gans (1995), Cretaceous to recent extension in the Bering Strait region, Alaska, *Tectonics*, 14(3), 549-563.

Ekstrom G., and E. R. Engdahl (1989), Earthquake source parameters and stress distribution in the Adak Island region of the central Aleutian Islands, Alaska, *J. Geophys. Res., 94*, 15,499-15,519.

Engdahl, E. R., S. Billington and C. Kisslinger (1989), Teleseismically recorded seismicity before and after the May 7, 1986, Andreanof Islands, Alaska, earthquake, *J. Geophys. Res., 94*, 15,481-15,498.

Engdahl, E. R., and D. Gubbins (1987), Simultaneous travel time inversion for earthquake location and subduction zone structure in the central Aleutian Islands, *J. Geophys. Res., 92*, 13,855-13,862.

Fletcher, H. J. (2002), Crust al Deformation in Alaska Measured Using the Global Positioning System, A Dissertation for the University of Alaska Fairbanks.

Fletcher, H. J., J. Beavan, J. Freymueller, L. Gilbert (2001), High interseismic coupling of the Alaska subduction zone SW of Kodiak island inferred from GPS data, Geophys. Res. Lett., 28(3), 443-446, 10.1029/2000GL012258.

Fournier, T., and J. T. Freymueller (2007), Transition from locked to creeping in the Shumagin Region, Alaska, *Geophys. Res. Lett.,* In press.

Freymueller, J. T., and J. Beavan (1999), Absence of strain accumulation in the western Shumagin segment of the Alaska subduction zone, *Geophys. Res. Lett., 26*, 3233-3236.

Freymueller, J. T., S. C. Cohen, and H. J. Fletcher (2000), Spatial variations in present-day deformation, Kenai Peninsula, Alaska, and their implications, *J. Geophys. Res.,105*, 8079-8101.

Fujita, K., K. G. Mackey, R. C. McCaleb, L. V. Cunbina, V. N. Kkovalev, V. S. Imaev, and V. N. Smirnov (2002), Seismicity of Chukotka, northeastern Russia, in: Tectonic evolution of the Bering shelf-Chukchi Sea-Arctic margin and adjacent landmasses, ed. By Miller, E. L., A. Grantz, and S. L. Klemper, *Geol. Soc. Amer. Spec. Pap.*, 360, 259-272.

Geist, E. L., J. R. Childs, and D. W. Scholl (1988), The origin of summit basins of the Aleutian ridge: Implications for block rotation of an arc massif, *Tectonics*, 7(2), 327-341.

Heki, K., S. Miyazaki, H. Takahashi, M. Kasahara, F. Kimata, S. Miura, N. F. Vasilenko, and A. Ivashchenko (1999), The Amurian Plate motion and current plate kinematics in eastern Asia, *J. Geophys. Res.*, 104(B12), 29147-29156, 10.1029/1999JB900295.

Houston, H. and E. R. Engdahl (1989), A comparison of the spatio-temporal distribution of moment release for the 1986 Andreanof Islands earthquake with relocated seismicity, *Geophys. Res. Lett.*, *16*(12), 1421-1424.

Hudson, T. and G. Plafker (1978), Kigluiak and Bendeleben Faults, Seward Peninsula In: Johnson, K. M., ed., The United States Geological Survey in Alaska—Accomplishments during 1977, *U.S. Geol. Survey Circ.* 722B, B47-B50.

Kanda, R. V., and M. Simons (2006), Simple Elastic Dislocation Models for Interpreting Interseismic Deformation in Subduction Zones, *Eos Trans.* AGU, 87(52), Fall Meet. Suppl., Abstract T12C-02

Lander, A. V., B. G. Bukchin, A. V. Kiryushin, and D. V. Droznin (1996), The tectonic environment and source parameters of the Khailino, Koryakiya earthquake of March

8, 1991: Does a Beringia plate exist?: *Computational Seismology and Geodynamics*, 3, 80-96.

Mackey, K., K. Fujita, L. Gunbina, V. Kovalev, V. Imaev, B. Koz'min, and L. Imeava (1997), Seismicity of the Bering Strait region: Evidence for a Bering block, *Geology*, 25(11), 979-982.

Mann, D. and J. Freymueller (2003), Volcanic and tectonic deformation on Unimak Island in the Aleutian Arc, Alaska, *J. Geophys. Res., 108*(B2), 2108, doi:10.1029/2002JB001925.

Minster, J. B., T. H. Jordan, P. Molnar, and E. Haines (1974), Numerical modeling of instantaneous plate tectonics, *Geophys. J. R. Astr. Soc.*, 36, 541-576.

Okada, Y. (1992), Internal deformation due to shear and tensile faults in a half-space, *Bull. Seisl. Soc. Am., 82*(2), 1018-1040.

Page, R. A., N. N. Biswas, J. C. Lahr, and H. Pulpan (1991) Seismicity of continental Alaska, in Slemmons, D. B., E. R. Engdahl, M. D. Zoback, and D. D. Blackwell, eds, Neotectonics of North America: Boulder, Colorado, Geological Society of America, Decade Map Volume 1.

Page, R. A., G. Plafker, and H. Pulpan (1995), Block rotation in east-central Alaska: a framework for evaluating earthquake potential? *Geology,* 23, 629-632.

Ratchkovski, N., and R. Hansen (2002), New constraints on tectonics of interior Alaska: Earthquake locations, source mechanisms, and stress regime, *Bull. Seis. Soc. Am.,* 92(3), 998-1014.

Ryan, H. F., and D. W. Scholl (1989), The evolution of forearc structures along an oblique convergent margin, central Aleutian arc, *Tectonics*, 8(3), 497-516.

Savage, J. C. (1983), A dislocation model of strain accumulation and release at a subduction zone, *J. Geophys. Res.*, *88*, 4984-4996.

Sella, G. F., T. H. Dixon, and A. Mao (2002), REVEL; a model for recent plate velocities from space geodesy, *J. Geophys. Res., 107*(B4), doi:10.1029/2000JB000033.

Sella, G. F., S. Stein, T. H. Dixon, M. Craymer, T. S. James, S. Mazzotti, and R. K. Dokka (2007), Observation of glacial isostatic adjustment in "stable" North America with GPS, *Geophys. Res. Lett.*, 34, L02306, doi:10.1029/2006GL027081.

Turner D. L., and S. E. Swanson (1981), Continental rifting: A new tectonic model for the central Seward Peninsula, in Wescott, E., and D. Turner, eds., Geothermal

reconnaissance survey of the central Seward Peninsula, Alaska: Fairbanks, University of Alaska, *Geophysical Institute Report* 284, 7-36.

Williams, T. B., H. M. Kelsey, and J. T. Freymueller (2006), GPS-derived strain in northwestern California: Termination of the San Andreas fault system and convergence of the Sierra Nevada-Great Valley block contribute to southern Cascadia forearc contraction. *Tectonophysics*, 413, 171-184.

Watts, A. B., J. H. Bodine and M. S. Steckler (1980), Observations of flexure and the state of stress in the oceanic lithosphere. *J. Geophys. Res.*, 85 6369-76

Wells, R. E., C. S. Weaver, and R. J. Blakely (1998), Forearc migration in Cascadia and its neotectonic significance. *Geology* 26, 759-762.

Zweck, C., and J. T. Freymueller (2002), Three-dimensional elastic dislocation modeling of the postseismic response to the 1964 Alaska earthquake, *J. Geophys. Res.*, 107(B4) 10.1029/2001JB000409.

3.10 Appendices

Appendix 3.1 Station locations and velocities (mm/yr). Velocities are relative to North America, ±1σ uncertainties are shown for the east, north and vertical components.

Station	Longitude	Latitude	East	North	Vertical	E_σ	N_σ	V_σ
Andreanof Islands Stations								
AT18	-176.64	51.86	-9.50	6.52	9.13	0.64	0.47	1.21
ATKA	-174.21	52.22	-1.94	-3.98	-0.84	0.26	0.28	0.48
BED1	-176.64	51.88	-8.29	6.47	4.91	0.30	0.29	0.55
BETT	-176.64	51.82	-9.18	6.46	5.55	0.65	0.47	1.34
BR6	-176.67	51.87	-10.17	5.38	5.53	4.04	1.54	4.21
BUGS	-176.63	51.85	-8.42	6.54	7.20	0.50	0.41	1.01
CHUN	-174.25	52.18	-3.93	-3.05	1.38	0.61	0.47	1.22
CLUB	-176.64	51.85	-8.91	6.37	9.58	0.48	0.39	0.96
DEC2	-174.17	52.23	-2.93	-3.44	4.46	0.84	0.51	1.53
FNGB	-176.63	51.83	-9.31	6.98	7.42	0.58	0.43	1.15
GATE	-177.15	51.85	-7.75	6.22	10.63	0.47	0.38	0.93
J122	-176.64	51.88	-9.60	6.53	4.20	2.64	1.46	3.63
KICM	-177.20	51.92	-7.37	7.42	0.64	3.95	2.30	5.44
KIRH	-177.09	51.90	-7.54	6.95	1.20	0.81	0.59	1.59
LORA	-176.62	51.99	-6.65	6.77	5.02	0.65	0.48	1.32
MIDK	-177.24	51.76	-9.17	7.52	7.29	0.41	0.35	0.81
PUPA	-174.24	52.20	-3.41	-3.01	5.21	0.72	0.54	1.43
ROE2	-177.12	51.76	-8.55	7.99	8.19	0.39	0.34	0.74
SHTG	-176.60	51.94	-8.60	6.33	11.88	0.48	0.39	0.96
WABM	-176.71	51.87	-8.03	6.00	7.32	0.32	0.31	0.60
WNDA	-174.29	52.16	-3.09	-2.52	1.27	0.78	0.58	1.59
ZETP	-176.56	51.93	-6.88	5.83	4.54	0.62	0.45	1.22
Fox Islands Stations								
AKHB	-165.73	54.10	-1.84	-3.72	0.83	0.62	0.48	1.29
AKPS	-165.85	54.15	0.25	-3.74	1.96	0.43	0.37	0.89
AKSO	-165.94	54.14	-0.91	-3.18	-4.68	1.02	0.67	2.19
BROD	-165.87	54.11	-0.62	-5.24	0.71	0.63	0.48	1.27
DCH1	-166.53	53.89	-2.30	-2.82	2.07	0.14	0.24	0.23
GUNN	-166.52	53.92	-2.10	-3.93	4.44	0.35	0.33	0.71
ILIU	-166.48	53.85	-1.82	-3.83	3.06	0.41	0.35	0.84
ROWD	-168.85	52.97	-7.44	-2.97	8.69	0.83	0.60	1.71
SBS2	-166.52	53.90	-1.66	-2.42	3.37	1.29	1.05	2.80
UNAL	-167.75	53.34	-4.59	-0.20	-2.23	0.77	0.59	1.63

Alaska Peninsula Stations								
ASPE	-157.37	56.85	-6.32	4.63	-2.82	2.33	1.66	4.77
CHIR	-155.73	55.83	-17.28	32.87	-10.58	0.74	0.55	1.51
CHNB	-159.58	54.81	-4.82	3.26	-0.50	6.53	3.10	8.99
CHRN	-162.37	54.63	-4.51	-3.83	1.54	1.40	1.02	2.97
CLFF	-158.30	56.21	-8.17	4.42	-6.48	2.38	1.66	4.85
CROW	-162.80	54.49	-3.23	-3.50	3.85	0.39	0.34	0.73
DAY	-162.47	54.74	-2.36	-0.65	2.09	2.31	1.62	4.54
FAWN	-162.36	54.82	0.28	-4.60	2.95	1.98	1.41	4.12
HEID	-158.61	56.96	-5.90	1.33	2.81	0.66	0.49	1.27
HUEY	-156.86	56.79	-9.47	5.19	4.57	3.28	2.29	5.86
ISLK	-158.60	56.11	-9.01	4.26	-3.01	2.48	1.83	5.60
KATY	-163.52	55.04	-1.73	-2.69	0.29	0.44	0.36	0.86
LAG	-162.30	54.66	-0.10	-2.44	1.94	3.03	2.23	6.32
LONE	-162.00	54.76	-2.07	-2.63	2.46	2.42	1.69	4.87
PANK	-163.11	54.68	-3.18	-2.35	4.42	0.82	0.61	1.71
PETE	-162.62	54.38	-2.78	-3.28	2.06	0.29	0.29	0.57
REEF	-162.52	54.86	-2.07	-2.61	3.26	1.97	1.45	4.19
SATT	-162.73	55.17	-2.25	-3.53	1.16	0.63	0.50	1.26
SEMI	-156.69	56.05	-12.35	14.79	6.81	2.36	1.62	4.64
SENI	-160.14	56.40	-5.48	-0.73	5.78	1.26	0.86	2.59
SMNF	-159.27	54.90	-11.45	8.31	-2.62	1.39	0.79	2.21
SNDP	-160.48	55.35	-7.58	2.19	0.90	0.56	0.40	1.00
STAR	-159.17	55.89	-9.61	4.74	5.46	2.38	1.57	4.48
TELE	-162.60	54.98	-3.58	-3.39	1.09	1.41	1.00	2.96
VSG	-159.09	56.12	-7.96	4.76	1.09	1.07	0.76	2.25
WIK	-157.11	56.58	-8.56	7.97	1.98	3.65	2.55	6.57
YAST	-159.42	56.39	-5.87	1.20	3.47	1.26	0.91	2.65
Bering Plate Interior Stations								
ELIB	-162.27	64.61	1.39	-4.70	10.89	7.09	3.48	9.38
GAMB	-171.73	63.77	-0.31	-5.29	-7.39	0.89	0.69	2.02
HOOP	-166.14	61.52	1.56	-3.45	-15.89	1.85	1.03	3.36
MELS	-163.69	64.92	-1.35	-5.41	1.14	1.18	0.88	2.56
OMEA	-165.44	64.51	3.31	-5.40	2.15	1.94	1.24	3.99
SPSW	-170.25	57.15	-1.08	-4.50	-7.50	0.64	0.51	1.26
Western Aleutian Stations (pre-2002 velocities)								
ANDY	173.18	52.88	-24.74	16.86	2.31	0.95	0.64	1.82
BKEB	179.28	51.38	-19.84	0.63	1.55	1.14	0.73	1.86
BKI	165.98	55.19	-33.74	36.29	1.88	0.20	0.24	0.23
BR2	174.10	52.72	-20.31	11.22	3.12	0.85	0.62	1.71
GEO1	173.18	52.85	-27.86	14.34	3.35	0.86	0.58	1.63
MURD	173.17	52.80	-27.38	14.46	1.96	0.39	0.33	0.70
NO17	173.18	52.83	-26.17	4.36	6.70	3.32	2.02	6.28

SIDE	173.19	52.86	-20.94	14.62	7.80	1.52	1.15	3.62
WALT	173.18	52.87	-27.16	13.78	2.35	0.76	0.51	1.43
Eastern Russia stations								
ANAD	177.50	64.74	5.85	3.06	-1.42	1.08	0.86	2.57
BILI	166.44	68.08	2.60	-1.48	0.74	0.15	0.23	0.14
KMS	166.21	62.46	2.33	-0.35	9.44	0.16	0.23	0.14
TIL	166.15	60.45	-3.11	-6.96	-9.51	0.17	0.23	0.15
Interior Alaska Stations (pre-2002 velocities)								
ATT	-145.85	63.50	-1.16	-0.15	-1.33	0.98	0.71	2.11
BRWN	-149.29	64.17	0.42	-4.67	-6.03	1.43	0.77	2.86
BSB4	-145.79	63.91	1.79	-1.27	0.84	0.74	0.56	1.61
CENA	-144.68	65.50	1.40	-1.49	-1.43	0.13	0.21	0.22
CLGO	-147.86	64.87	1.46	-2.59	-0.47	0.10	0.21	0.15
EGL2	-145.39	65.49	-0.55	-1.68	-7.30	1.61	1.18	3.40
GRNR	-148.98	63.84	0.75	-1.87	2.83	0.14	0.22	0.24
MINT	-148.90	65.10	0.92	-3.45	6.53	0.77	0.62	1.64
ORTT	-141.94	62.96	4.21	-1.57	2.94	2.05	1.24	3.73
PPLN	-145.85	64.15	-0.32	-3.12	-2.60	0.72	0.56	1.52
SATT	-162.73	55.17	-1.36	-3.36	1.21	0.57	0.46	1.14
SLCH	-146.98	64.48	0.79	-2.61	0.49	0.42	0.35	0.86
STRI	-142.95	63.33	0.67	-3.79	5.19	1.42	0.91	2.81
TOLO	-149.50	65.05	2.34	-2.34	-8.66	1.56	1.19	3.36
WOND	-150.87	63.49	3.15	-8.69	0.64	0.89	0.65	1.92

Appendix 3.2 Fault plane parameters used for dislocation modeling. The longitude and latitude describe the southeastern most corner of each plane. Depth is the vertical distance to the top of each plane. Length, width and depth are in units of kilometers, strike and dip are in unit of degrees, the strike direction is listed such that dip is "down to the right." Coupling is the best value of coupling and 95% range is the range of coupling at the 95% confidence limits and within the realistic physical values.

Name	Long	Lat	Length	Width	Dip	Strike	Depth	Coupling	95% range
Andreanof Islands region									
Adak upper	-174.95	50.42	354.1	57.6	8.0	172.4	7	13%	0 to 100%
Adak middle	-174.29	50.99	407.8	37.3	20.4	172.2	15	100%	59 to 100%
Adak lower	-175.08	51.24	355.0	40.7	27.8	172.6	28	100%	75 to 100%
Adak bottom	-175.15	51.66	354.8	32.4	38.7	172.8	54	-27%	-61 to 2%
Atka upper	-171.83	50.67	223.3	57.6	8.0	170.2	7	79%	0 to 100%
Atka middle	-171.92	51.18	167.4	37.3	20.4	170.2	15	0%	0 to 80%
Atka lower	-171.99	51.49	217.3	40.7	27.8	170.1	28	25%	0 to 65%
Atka bottom	-172.06	51.91	215.1	32.4	38.7	170.3	54	11%	0 to 100%
Fox Islands region									
Fox 1	-162.93	53.09	436.0	50.0	7.0	156.2	7	100%	70 to 100%
Fox 2	-163.22	53.53	240.0	45.0	20.0	155.8	14	90%	80 to 100%
Fox 3	-166.53	52.68	197.0	43.0	20.0	155.8	14	100%	80 to 100%
Fox 4	-163.48	53.91	436.0	49.0	23.0	154.8	30	10%	0 to 20%
Fox 5	-163.83	54.38	436.0	45.0	32.0	152.0	47	0%	0 to 15%
Alaska Peninsula region									
AK Pen. 4	-152.24	55.50	216.9	216.7	7.9	150.3	5	89%	63 to 94%
AK Pen. 3	-155.34	54.70	189.1	179.4	9.8	151.3	5	70%	24 to 92%
AK Pen. 2	-157.99	54.00	125.3	168.3	11.0	152.3	5	30%	9 to 57%
AK Pen. 1	-159.78	53.60	154.9	91.5	12.7	153.3	5	0%	0 to 73%
Near Islands region									
Near Islands	174.40	51.20	300.0	120.0	14.0	210.0	5	62%	40 to 82%

Chapter 4

Conclusions

4.1 Tectonic Summary

The Bering plate does exist. Our GPS measurements have allowed a quantitative analysis that places an Euler pole for the plate at 42.5° N, 121.3° E with an angular velocity of 6.0°/my relative to the North American plate. Given the boundaries of the plate, this pole indicates that most of the plate moves in a general southward direction resulting in extension on the Seward Peninsula and a southward migrating Aleutian subduction zone. The eastern boundary of the Bering plate is not clearly defined and may be very diffuse. We have speculated that the seismicity in interior Alaska is partially driven by a Bering plate that is moving relative to the North American plate lying farther to the east.

Some of the most interesting findings of this study relate to translation of the Aleutian arc, a subject that has been speculated on for decades but has not been easy to quantitatively assess. We used direct GPS measurements, elastic dislocation modeling results and slip vector azimuths to study slip partitioning and arc dismemberment. We find that slip partitioning is present in the forearc throughout the Aleutians, but slip partitioning in the back-arc only develops west of Amchitka Pass where subduction becomes very oblique.

We developed elastic dislocation models primarily to determine arc translation velocities throughout the arc for analyzing the motion of the Bering plate, but in the

process also learned much more about the subduction zone behavior. In the central Aleutians, we developed an accurate fault plane model based on carefully relocated seismicity. We found that along strike variations in GPS derived velocities are explained completely by along strike variations in coupling. More specifically, the thrust interface in the western Andreanof region, which has experienced several very large earthquakes in the last 50 years, is entirely locked, whereas the eastern region is slipping freely and causes no strain in the overriding plate. This eastern region has experienced much less slip in earthquakes than the western region. Similar dramatic variations in coupling have been uncovered in the subduction zone along the Alaska Peninsula. We have revealed the primary tectonic setting of the Bering Sea area and set the stage for many more detailed studies.

4.2 Societal Impact

As more and more GPS measurements are made throughout the Aleutians, we will soon be able to give a first order approximation of coupling for the entire subduction interface. This is important for recognizing regions with the greatest seismic hazard, and has far-reaching affects as tsunamis generated in the Aleutians can impact regions all around the Pacific Ocean. Furthermore, understanding interseismic strain accumulation and postseismic deformation in the Aleutians allows for better measurements of volcanic deformation. GPS measurements are becoming more important in volcano monitoring and are important in recognizing inflation preceding eruptions. Eruptions in the Aleutians must be carefully monitored, as this is a major international air traffic route.

This study has identified a plate boundary zone in western Alaska, a region previously considered to lie within the interior of the North American plate. This recognition may call for a reassessment of seismic hazard in western Alaska. Regions with high strain rates and active seismicity need to be considered carefully with regard to the development of buildings and infrastructure. With the identification of another plate boundary comes the need for improved and increased geophysical monitoring.